Model peptide for anti-sigma factor domain HHCC zinc fingers: high reactivity toward 1O2 leads to domain unfolding

Valentin Chabert, Vincent Lebrun, Colette Lebrun, Jean-Marc Latour, Olivier Sénèque

Chemical Science

EDGE ARTICLE

Cite this: *Chem. Sci.*, 2019, **10**, 3608

All publication charges for this article have been paid for by the Royal Society of Chemistry

Model peptide for anti-sigma factor domain HHCC zinc fingers: high reactivity toward $^1O_2$ leads to domain unfolding†

Valentin Chabert, ‡[a] Vincent Lebrun,‡[a] Colette Lebrun, [b] Jean-Marc Latour [a] and Olivier Sénèque *[a]

Received 21st January 2019
Accepted 14th February 2019

DOI: 10.1039/c9sc00341j

rsc.li/chemical-science

All organisms have to cope with the deleterious effects of reactive oxygen species. Some of them are able to mount a transcriptional response to various oxidative stresses, which involves sensor proteins capable of assessing the redox status of the cell or to detect reactive oxygen species. In this article, we describe the design, synthesis and characterization of Zn·L_{ASD}(HHCC), a model for the $Zn(Cys)_2(His)_2$ zinc finger site of ChrR, a sensor protein involved in the bacterial defence against singlet oxygen that belongs to the family of zinc-binding anti-sigma factors possessing a characteristic H/C–$X_{24/25}$–H–X_3–C–X_2–C motif. The 46-amino acid model peptide L_{ASD}(HHCC) was synthetized by solid phase peptide synthesis and its Zn^{2+}-binding properties were investigated using electronic absorption, circular dichroism and NMR. L_{ASD}(HHCC) forms a 1 : 1 complex with Zn^{2+}, namely Zn·L_{ASD}(HHCC), that adopts a well-defined conformation with the Zn^{2+} ion capping a 3-helix core that reproduces almost perfectly the fold of the ChrR in the vicinity of its zinc site. H_2O_2 reacts with Zn·L_{ASD}(HHCC) to yield a disulfide with a second order rate constant of 0.030 ± 0.002 M^{-1} s^{-1}. Zn·L_{ASD}(HHCC) reacts rapidly with singlet oxygen to yield sulfinates and sulfonates. A lower limit of the chemical reaction rate constant between Zn·L_{ASD}(HHCC) and $^1O_2$ was determined to be 3.9 × 10^6 M^{-1} s^{-1}. Therefore, the $Zn(Cys)_2(His)_2$ site of Zn·L_{ASD}(HHCC) appears to be at least 5 times more reactive toward these two oxidants than that of a classical ββα zinc finger. Consequences for the activation mechanism of ChrR are discussed.

Introduction

Organisms living in an aerobic environment have to cope with the deleterious effects of oxidative stress, which is caused by a family of molecules produced from dioxygen in the living cell, the so-called Reactive Oxygen Species (ROS).[1] ROS are classified into two categories according to their production pathways: Type I for those arising from electron(s) addition to O_2 (*e.g.*: superoxide anion $O_2^{\bullet-}$, hydrogen peroxide H_2O_2, hypochlorous acid HOCl, hydroxyl radical HO$^\bullet$…) and Type II for electronically excited states of dioxygen arising from a physical activation of the ground (triplet) state ($^3O_2$).[2–4] The lowest energy excited state of O_2, commonly called singlet oxygen ($^1O_2$), is produced mainly in photosynthetic organisms. These organisms, as well as others like mammalians, have been shown to elicit a specific response to $^1O_2$, demonstrating that sensing pathways exist for this ROS.[5–7] One of the best characterized is that of *Rhodobacter sphaeroides*. It involves the protein σ^E, a group IV sigma factor up-regulating the expression of the response against $^1O_2$ stress.[8–11] σ^E is negatively regulated by its cognate anti-sigma factor, ChrR. In normal conditions, the anti-sigma factor sequesters its cognate sigma factor (Fig. 1A). Under $^1O_2$ stress, the anti-sigma factor undergoes a structural change and releases its sigma factor, which can then bind RNA polymerase, up-regulating the expression of specific genes involved in the response to $^1O_2$ stress. The anti-sigma factor interacts with the sigma factor mainly *via* its N-terminal domain, named anti-sigma factor domain (ASD).[10] It is estimated that 33% of the group IV sigma factors are regulated by an anti-sigma factor containing an anti-sigma factor domain. Among the predicted cytoplasmic group IV anti-sigma factors, 92% contain a conserved zinc binding motif H–X_3–C–X_2–C, classifying them in the zinc-binding anti-sigma factor (ZAS) subfamily.[8]

In 2011, Andreini *et al.* classified 93% of the 15 763 known structures of protein zinc sites into a minimum set of structural motifs.[12] The two existing structures of ChrR[10] could not enter in any of the families defined by Andreini, which demonstrates the singularity of the zinc finger site of their anti-sigma factor domain. ChrR contains an anti-sigma factor domain featuring

[a]*Univ. Grenoble Alpes, CNRS, CEA, BIG, LCBM (UMR 5249), F-38000 Grenoble, France. E-mail: olivier.seneque@cea.fr*

[b]*Univ. Grenoble Alpes, CEA, CNRS, INAC-SyMMES, F-38000 Grenoble, France*

† Electronic supplementary information (ESI) available: Experimental details for peptide synthesis and characterization, absorption and circular dichroism analyses of Zn^{2+} binding, H_2O_2 oxidation, $^1O_2$ oxidation and solution structure determination by NMR. See DOI: 10.1039/c9sc00341j

‡ These authors contributed equally to this work.

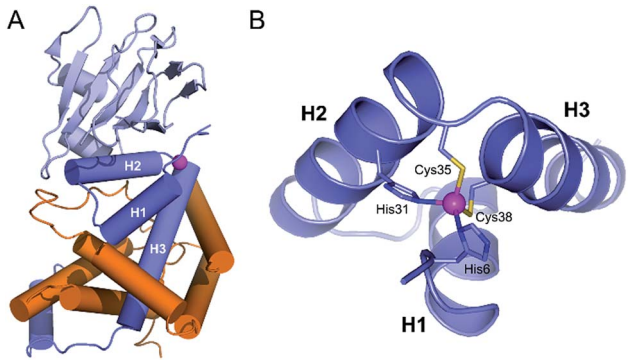

Fig. 1 (A) Crystallographic structure of the ChrR–σ^E complex (pdb 2Z2S)[8] showing the sigma factor σ^E in orange and the anti-sigma factor ChrR in blue with anti-sigma factor domain in dark blue and cupin-like domain in light blue. The zinc ion is shown in magenta. (B) View of the anti-sigma factor domain zinc finger site embedded within helices H1, H2 and H3, showing Zn^{2+}-binding histidines and cysteines of the H–X_{24}–H–X_3–C–X_2–C motif.

a HHCC zinc finger site with a H–X_{24}–H–X_3–C–X_2–C motif (Fig. 1B). Interestingly, RslA and RsrA, two ChrR homologs featuring also a zinc finger site – HHCC within a H–X_{24}–H–X_3–C–X_2–C motif for RslA[13] and CHCC within a C–X_{25}–H–X_3–C–X_2–C motif for RsrA[14] – are sensitive to oxidative conditions and trigger a response against oxidative stress.[13–16] Noteworthy, the zinc site of RsrA is described as a redox switch, acting as a detection module for disulfide stress. A similar role was proposed for the zinc site of RslA to sense oxidative stress.[13–16] It has been proposed that the oxidation of the ZAS protein zinc finger induces Zn^{2+} release and unfolding of the anti-sigma factor domain, leading to dissociation of the ZAS protein from its cognate sigma factor. However, it was recently demonstrated that oxidation of zinc-binding cysteine of the ZAS zinc finger is not always sufficient to dissociate the anti-sigma factor–sigma factor complex.[17] Similarly, it has been hypothesized that the zinc site of ChrR could sense $^1O_2$ *via* zinc-bound thiol oxidation inducing dissociation of the anti-sigma factor domain from σ^E, which is supported by the demonstration that (i) formation of the zinc finger site in the N-ter domain anti-sigma factor domain of ChrR is essential for the ChrR–σ^E complex formation, and (ii) the Zn-loaded anti-sigma factor domain alone is sufficient to sequester σ^E. Additionally, it was also shown that the C-terminal cupin-like domain of ChrR is required for $^1O_2$ response *in vivo*,[10,11] but there is no data ruling out the involvement of the zinc finger site – and its oxidation – in these studies. The full mechanism of activation of ChrR by $^1O_2$ remains to be elucidated.

We have previously shown that small metallopeptides modelling zinc finger sites are useful tools to gain interesting insights into the reactivity of zinc fingers toward ROS at the molecular level (oxidation products, kinetic rates).[18–20] In particular, we have shown that a $Zn(Cys)_4$ zinc finger of the treble clef family of zinc fingers could be efficiently oxidized by $^1O_2$ [21] whereas $^1O_2$ oxidation of the $Zn(Cys)_2(His)_2$ site of classical ββα zinc fingers is far less efficient.[22] This questions the role of the $Zn(Cys)_2(His)_2$ zinc finger in ChrR. To address this question, we developed a 46-amino acid peptide modelling the anti-sigma factor domain zinc finger site of ChrR and we studied its reactivity towards H_2O_2 and $^1O_2$. We show that its oxidation leads to Zn^{2+} release and peptide unfolding. Remarkably, the cysteines of this uncommon $Zn(Cys)_2(His)_2$ site found in ZAS are rapidly oxidized by $^1O_2$ compared to classical ββα zinc fingers, in agreement with their putative involvement in $^1O_2$ detection.

Results

Peptide design

To date, two crystal structures of anti-sigma factor domain-containing proteins displaying a zinc finger site (HHCC type) have been elucidated: ChrR[10] and RslA.[13] Anti-sigma factor domains display four α-helices and among them, three are involved in the constitution of the zinc finger site, which is displayed in Fig. 1B. These three helices (H1, H2 and H3) are held together by the chelation of a Zn^{2+} ion and by closely packed hydrophobic side chains within the heart of the 3-helix core. Helices H2 and H3 (Fig. 1B) form a knuckle bearing the H–X_3–C–X_2–C conserved motif, coordinating the Zn^{2+} ion. The fourth zinc ligand is a histidine residue located at the N-terminus resulting in an overall H–X_{24}–H–X_3–C–X_2–C Zn^{2+}-binding motif (Fig. 2). In order to reproduce the reactivity of a given zinc finger site, it is important to perfectly reproduce the various features of the site that can influence its reactivity. This includes the coordination sphere of the Zn^{2+} ion, the folding of the peptide around and the hydrogen bonds that are established with the Zn^{2+}-bound sulfurs.[18,20,23] It has been shown with RsrA that the anti-sigma factor domain can adopt different folds depending whether it is bound to its sigma-factor or not.[17] Since our aim is to better understand if the reactivity of ChrR's zinc site could play a role in the sensing of $^1O_2$, we aim here at reproducing the fold as complexed with σ^E. Hydrophobic cores proximal to the zinc finger site can be important to enhance Zn^{2+} affinity to the model peptide and to ensure its proper folding.[24] For these reasons, we decided to include the three helices in our model.

The design of the model peptides was based on the sequence and X-ray crystallographic structure of ChrR anti-sigma factor domain (Fig. 2),[10] which was re-engineered as follows. (i) In the HH motif present at the N-terminus, only the second residue is involved in Zn^{2+} coordination as part of the canonical H–X_{24}–H–X_3–C–X_2–C motif. In order to avoid scrambling of Zn^{2+} ligand, the first histidine of the HH motif was changed for a lysine. (ii) Helices H1, H2 and H3 present several hydrophobic side chains

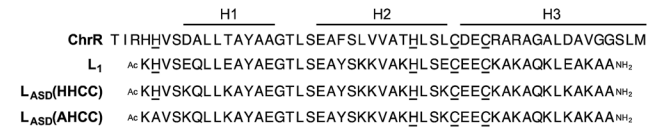

Fig. 2 Sequence alignment of the N-terminal domain of ChrR (top) and the model peptides presented in this article, Zn^{2+}-binding amino acids underlined.

that point toward the exterior of the structure because they are involved in the interaction with the sigma factor σ^E. In order to favour the correct fold of our model peptide and to ensure solubility, these hydrophobic amino acids were randomly changed for polar amino acids (E, Q or K). (iii) As β-branched amino acids such as threonine or valine may destabilize α-helices,[25] two threonines located in helices H1 and H2, and pointing toward the exterior of the structure were changed for lysines. Similarly, glycines in helix H3, which may destabilize a helical fold, were changed for glutamine and alanines. (iv) The C-terminus of the peptide was amidated to remove the carboxylate charge that could destabilize the C-terminus of helix H3.[26] (v) Non-essential aspartates and arginines were changed for glutamates and lysines to avoid side reactions during solid phase peptide synthesis (SPPS) and maximize synthesis yields. This led to peptide L_1, whose sequence is displayed in Fig. 2. As a first try to model the anti-sigma factor domain zinc finger, this 46-amino acid peptide was synthetized by SPPS. Unfortunately, when dissolved in various buffers at pH around 7, L_1 precipitated when Zn^{2+} was added. Mapping charged amino acids of the L_1 sequence onto the 3-helix motif of ChrR using Pymol[27] revealed that most of the negatively charged glutamate residues are clustered on one face of the structure whereas positively charged lysines are clustered on another face. Suspecting that this could be the reason for precipitation of the Zn^{2+} complex, the charged amino acids were re-distributed in the sequence for random disposition onto the 3-helix surface. This led to peptide L_{ASD}(HHCC) (Fig. 2), which was synthetized by SPPS. Note that four pseudoproline dipeptides[28] were used to avoid aggregation of the elongating chain during synthesis (see ESI† for details).

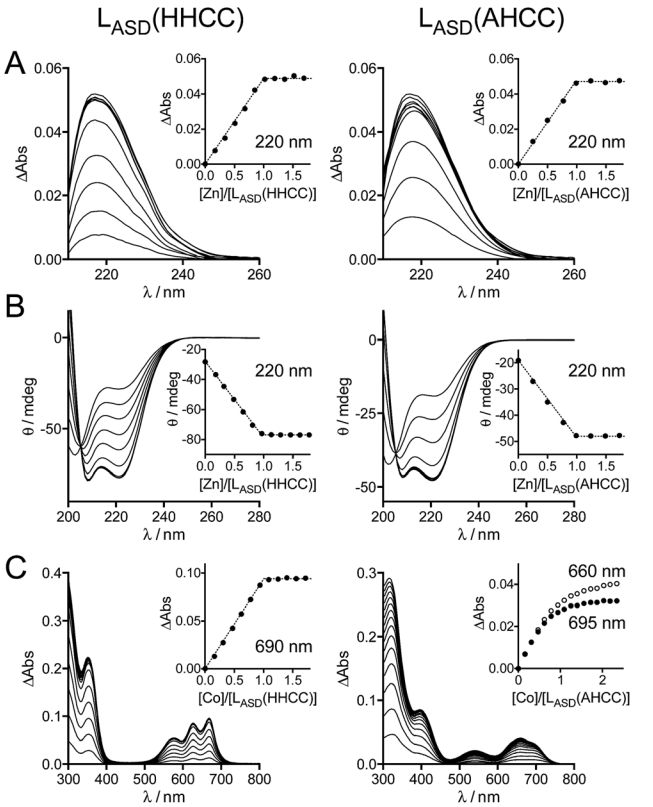

Fig. 3 UV-Vis absorption and CD characterization of L_{ASD}(HHCC) and L_{ASD}(AHCC). (A) Absorption and (B) CD monitoring of Zn^{2+} titrations of L_{ASD}(HHCC) (19 μM, left) and L_{ASD}(AHCC) (14 μM, right) in phosphate buffer (20 mM, pH 7.0) containing TCEP (500 μM) with inserts showing the evolution of the absorbance at 220 nm. For absorption, the spectrum of the metal-free peptide was subtracted from each spectrum. (C) Absorption monitoring of Co^{2+} titrations of L_{ASD}(HHCC) (153 μM, left) and L_{ASD}(AHCC) (110 μM, right) in phosphate buffer (20 mM, pH 7.0) containing TCEP (500 μM) with inserts showing the evolution of the absorbance at 690 nm for L_{ASD}(HHCC) and 660 and 695 nm for L_{ASD}(AHCC).

Zinc binding and folding properties

The metal binding properties of L_{ASD}(HHCC) were investigated by combination of UV-Vis absorption, circular dichroism (CD) and NMR. Titrations monitored by UV absorption were used to determine the stoichiometry of the peptide–metal complexes. Upon addition of Zn^{2+} in a buffered peptide solution, an increasing absorption band is observed at *ca.* 220 nm, which corresponds to $Cys \cdot S^- \rightarrow Zn^{2+}$ ligand-to-metal charge transfer (LMCT) transitions (Fig. 3A).[24] This signal increases linearly up to one equivalent of zinc and plateaus afterwards (inserts Fig. 3A). This indicates the formation of a 1 : 1 complex only, *i.e.* $Zn \cdot L_{ASD}$(HHCC). The intensity of this band is $\Delta\varepsilon = 6600\ M^{-1}\ cm^{-1}$, which is in agreement with two zinc-bound cysteinates.[20,24,29] To gain further insight into the coordination sphere of the Zn^{2+} ion, L_{ASD}(HHCC) was titrated with Co^{2+}, a Zn^{2+} ion surrogate commonly used to probe its geometry and coordination sphere. Absorption bands characteristic of $Cys \cdot S^- \rightarrow Co^{2+}$ LMCT (in the range 220–400 nm) and d–d (in the range 500–700 nm) transitions appear upon coordination of Co^{2+} by L_{ASD}(HHCC) (Fig. 3C). Similarly to the Zn^{2+} titration, only the 1 : 1 $Co \cdot L_{ASD}$(HHCC) complex is detected. The wavelengths (576, 627 and 670 nm) and intensity ($\varepsilon = 620\ M^{-1}\ cm^{-1}$ at 627 nm, *i.e.* $\varepsilon > 300\ M^{-1}\ cm^{-1}$) of the d–d transitions are in agreement with a tetrahedral $Co(Cys)_2(His)_2$ site.[20,24,30,31] From these data, we can reasonably infer the formation of a tetrahedral 1 : 1 $Zn \cdot L_{ASD}$(HHCC) complex with $(Cys)_2(His)_2$ coordination. Thereafter, the folding of the peptide was investigated by CD (Fig. 3B). The CD spectrum of the metal-free L_{ASD}(HHCC) shows an intense negative signal with minimum at *ca.* 200 nm and a shoulder at *ca.* 222 nm. This corresponds to a random coil peptide with a small content of helical fold. In agreement with absorption studies, upon titration of L_{ASD}(HHCC) by Zn^{2+}, evolution of the CD spectrum is observed up to 1 eq. Zn^{2+} with a clean isodichroic point at 205 nm, thereby confirming the formation of a complex with 1 : 1 stoichiometry only. The spectrum of $Zn \cdot L_{ASD}$(HHCC) is characteristic of a peptide with major helix content, as expected for this model. In order to determine the Zn^{2+} binding constant of L_{ASD}(HHCC) at pH 7.0, $K_{ZnL_{ASD}(HHCC)} = [Zn \cdot L_{ASD}(HHCC)]/([Zn^{2+}][L_{ASD}(HHCC)])$, CD titrations were performed in competition with EDTA and TPEN (1 eq.), two high-affinity Zn^{2+} chelators ($K_{ZnEDTA} = 10^{13.1}\ M^{-1}$ and $K_{ZnTPEN} = 10^{14.9}\ M^{-1}$ at pH 7.0). In the case of EDTA, *ca.* 95% of Zn^{2+} is bound to L_{ASD}(HHCC) after addition of 1.0 eq. Zn^{2+} *vs.* peptide (ESI†), indicating that

L_{ASD}(HHCC) binds Zn^{2+} tighter than EDTA but also that EDTA is not suitable for precise determination of the binding constant.[32,33] In the case of TPEN, we noticed a slow precipitation of the Zn^{2+}-free peptide in presence of this chelator, which precluded any competition experiment. Thus, only a lower estimate of the binding constant can be drawn from the EDTA competition, that is $K_{ZnL_{ASD}(HHCC)} \geq 10^{15.0}$ M^{-1}.

In order to confirm that the N-terminal histidine, which is remote from the core H–X_3–C–X_2–C binding motif in the sequence, is bound to the Zn^{2+} ion in our Zn·L_{ASD}(HHCC) model, a peptide variant with the N-terminal histidine replaced by an alanine, namely L_{ASD}(AHCC), was synthesized (Fig. 2 and ESI†). Upon Zn^{2+} titration, the formation of a 1 : 1 complex only is evidenced by both UV-Vis absorption and CD spectroscopies (Fig. 3A and B). The spectral features are very similar for both peptides, including LMCT absorption and CD spectra, either in their Zn-free and Zn-loaded forms. The intensity of the LMCT band ($\Delta\varepsilon = 8400$ M^{-1} cm^{-1}) is compatible with two zinc-bound cysteinates. Noteworthy, the CD spectrum of Zn·L_{ASD}(AHCC) is very similar to that of Zn·L_{ASD}(HHCC), indicating a similar helix content in the Zn-loaded form. Regarding Co^{2+} binding, analysis of the UV-Vis Co^{2+} titration of L_{ASD}(AHCC) shows a completely different d–d transition pattern compared to L_{ASD}(HHCC) with a two-step growing phase (the bands at 660 and 695 nm have the same intensity at the beginning of the titration (<0.5 eq.), then the band at 655 nm becomes the most intense, Fig. 3C), indicating the formation of both 2 : 1 and 1 : 1 Co/peptide species during the titration, with tetrahedral geometry as attested by the ε values above 300 M^{-1} cm^{-1} for the d–d transitions. Additionally, no plateau is observed after 1.0 eq., indicating a less stable 1 : 1 complex compared to Co·L_{ASD}(HHCC). Finally, the binding affinity of L_{ASD}(AHCC) for Zn^{2+} was assessed by competition with EDTA monitored by CD. When a 1 : 1 : 1 L_{ASD}(AHCC)/EDTA/Zn^{2+} mixture is prepared, *ca.* 25% of Zn^{2+} is bound to L_{ASD}(AHCC) *versus* 95% for L_{ASD}(HHCC) in the same conditions (ESI†). This corresponds to a value of *ca.* 10^{12} for $K_{ZnL_{ASD}(AHCC)}$, indicating that the replacement of the N-terminal histidine by an alanine lowers the Zn^{2+} affinity by at least 3 orders of magnitude.

Further insights into the structure of Zn·L_{ASD}(HHCC) and Zn·L_{ASD}(AHCC) were obtained by ^{1}H NMR. The 1D ^{1}H NMR spectra of metal-free L_{ASD}(HHCC) and L_{ASD}(AHCC) in H_2O/D_2O 9 : 1 display broad peaks with amide NH in the range 7.2–8.5 ppm indicating that these peptides are mostly random coil, in agreement with CD. Regarding Zn^{2+} complexes, the ^{1}H NMR spectrum of Zn·L_{ASD}(HHCC) displays sharp amide NH resonances spread over a wider range from 6.9 to 9.3 ppm (Fig. 4A, top, and ESI†). Many of them present $^3J_{HN,H\alpha} < 6$ Hz indicative of helical folding (Table S2 and Fig. S4 of ESI†). The 2D NOESY spectrum shows numerous correlation peaks corresponding to non-sequential NOEs that are characteristic of helical folding (Fig. S4 of ESI†). Additionally, several long-range NOEs between hydrophobic amino acid remote in the sequence indicate the formation of a hydrophobic core. This suggests the formation of a Zn^{2+} complex with a well-defined stable conformation. On the contrary, the ^{1}H NMR spectrum of Zn·L_{ASD}(AHCC) (Fig. 4A, bottom) shows very broad resonances in the amide NH region

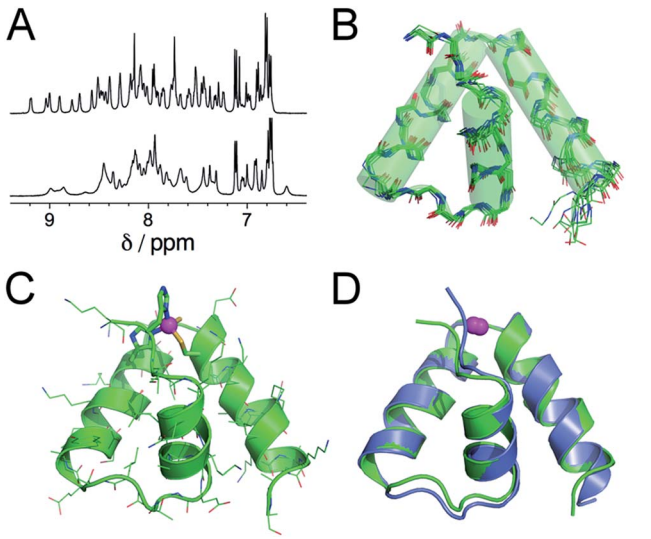

Fig. 4 (A) ^{1}H NMR spectra (500 MHz, H_2O/D_2O 9 : 1 pH 6.4, 298 K) of Zn·L_{ASD}(HHCC) (top) and Zn·L_{ASD}(AHCC) (bottom). (B) Superimposition of the 10 lowest energy structures of Zn·L_{ASD}(HHCC) calculated using X-PLOR with NMR-derived distance and dihedral angle constraints. (C) Lowest energy structure of Zn·L_{ASD}(HHCC). (D) Superimposition of the solution structure of Zn·L_{ASD}(HHCC) (green) and the corresponding sub-domain of the crystallographic structure of ChrR (blue, pdb 2Z2S).[10] The Zn^{2+} ion is shown in magenta.

although this complex displays a similar helix content as Zn·L_{ASD}(HHCC) as judged from its CD spectrum. This suggests a conformational equilibrium for Zn·L_{ASD}(AHCC). Indeed, the coordination of the N-terminal histidine to the Zn^{2+} ion is not necessary to fold the three helices, as indicated by CD but it plays a major role in freezing the conformation of the peptide in HHCC variant. Finally, the structure of Zn·L_{ASD}(HHCC) was calculated using X-PLOR with 466 H–H distance constraints (142 intraresidue, 138 sequential and 186 medium- and long-range) extracted from the NOESY spectrum and 35 ϕ dihedral constraints derived from $^3J_{HN,H\alpha}$ values. The superimposition of the ten lowest energy structures, which is depicted on Fig. 4B shows that Zn·L_{ASD}(HHCC) adopts a well-defined conformation with three helices (the backbone root mean square deviation over the ten structures is 0.83 Å). The zinc finger site caps this three-helix domain (Fig. 4C). The superimposition of the lowest energy structure of Zn·L_{ASD}(HHCC) with the zinc finger site taken from the crystallographic structure of ChrR anti-sigma factor domain (Fig. 4D) shows that the model reproduces almost perfectly the fold of the native protein, including helices H1, H2 and H3 as well as the loops between the helices. To summarize, L_{ASD}(HHCC) is able to bind only one Zn^{2+} ion to form a tetrahedral $Zn(Cys)_2(His)_2$ site that folds the peptide into a unique 3-helix conformation reproducing almost perfectly that of ChrR anti-sigma factor domain.

Oxidation of Zn·L_{ASD}(HHCC) by H_2O_2

The reactivity of Zn·L_{ASD}(HHCC) toward H_2O_2 and $^1O_2$ was investigated in order to assess the propensity of the anti-sigma factor domain zinc finger site to be oxidized by these two

oxidants in comparison with other zinc fingers. The reaction of $Zn\cdot L_{ASD}$(HHCC) (20 μM) with H_2O_2 (1 mM) in phosphate buffer (10 mM, pH 7.0) was monitored by CD (Fig. S3C of ESI†). This reaction is slow and after 15 h, the CD spectrum resembles that of zinc-free L_{ASD}(HHCC), indicating that the peptide unfolds upon reaction with H_2O_2. The product of the reaction was identified by ESI/MS as a disulfide (loss of two mass units). A similar CD spectrum was obtained by reacting $Zn\cdot L_{ASD}$(HHCC) with 2.5 eq. HOCl, a more efficient oxidant for zinc-bound thiolates known to form disulfides.[34] The kinetics of the reaction of $Zn\cdot L_{ASD}$(HHCC) with H_2O_2 at 298 K was determined using previously described procedures,[19] monitoring either the loss of the LMCT absorption in the UV or zinc release by using 4-(2-pyridylazo)resorcinol (PAR), which forms the $Zn(PAR)_2$ complex with intense absorption in the visible when Zn^{2+} is released from the peptide upon oxidation. The PAR assay is not recommended to follow the oxidation of $Zn(Cys)_3(His)$ or $Zn(Cys)_4$ because partially oxidized peptides displaying a reduced cysteine may retain Zn^{2+},[19] but for this $Zn(Cys)_2(His)_2$ zinc finger peptide, both methods gave the same result. In condition of excess H_2O_2, a mono-exponential evolution of the absorption signal (either LMCT or $Zn(PAR)_2$ band at 220 and 494 nm, respectively) is observed, indicating an apparent pseudo-first order reaction. Varying the concentration of H_2O_2 revealed a linear dependence on $[H_2O_2]$ of the apparent first-order rate constant k^{obs} (Fig. S3 of ESI†). Thus, the rate-determining step of the reaction is second order, first order in H_2O_2 and first order in $Zn\cdot L_{ASD}$(HHCC), as previously observed for other zinc fingers.[18–20] Indeed, the rate-determining step corresponds to the nucleophilic attack of H_2O_2 by the zinc-bound thiolate and its rate is given by $r = k \times [H_2O_2][Zn\cdot L_{ASD}(HHCC)]$ with $k = 0.030 \pm 0.002\ M^{-1}\ s^{-1}$ at 297 K.

Oxidation of $Zn\cdot L_{ASD}$(HHCC) by $^1O_2$

In previous studies,[21,22] we have shown that the reaction of $Zn(Cys)_4$ and $Zn(Cys)_2(His)_2$ zinc finger models with $^1O_2$ yields sulfinate species as major products, and disulfides in a lesser extent. Additionally, in a classical ββα $Zn(Cys)_2(His)_2$ zinc finger, Zn^{2+} coordination inhibits photooxidation of histidines. Oxidation of $Zn\cdot L_{ASD}$(HHCC) by $^1O_2$ was investigated as previously described for other $Zn(Cys)_4$ and $Zn(Cys)_2(His)_2$ zinc finger models:[21,22] the oxidation products were identified by combination of HPLC and ESI-MS analyses and the reaction rate was assessed in competition experiments with a reference compound. Rose bengal or methylene blue were used as photosensitizers to produce $^1O_2$ in this study. $Zn\cdot L_{ASD}$(HHCC) was photooxidized in D_2O buffered with phosphate or ammonium acetate. HPLC analyses were performed with acidic eluent (0.1% TFA) so that Zn^{2+} is removed from the peptide during analysis. The HPLC chromatogram of a solution of $Zn\cdot L_{ASD}$(HHCC) containing the photosensitizer but maintained in the dark showed a single peak at $t_R = 20.3$ min corresponding to the reduced peptide L_{ASD}(HHCC) (Fig. 5B). Upon irradiation, a second peak appears at a shorter retention time ($t_R = 18.1$ min). Prolongated irradiation shows an increase of the peak at 18.1 min at the expense of the one at 20.3 min. The main product detected

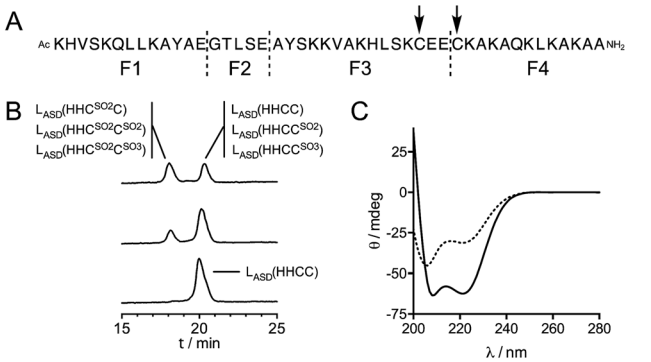

Fig. 5 (A) GluC digestion sites (dashed lines) and $^1O_2$ oxidation sites (arrows) identified for L_{ASD}(HHCC). (B) HPLC chromatograms obtained before (bottom) and after 1 min (middle) and 5 min (top) irradiation of a solution of $Zn\cdot L_{ASD}$(HHCC) (60 μM) containing rose bengal (2 μM), in 20 mM Pi (D_2O pD 7.0). The species identified by digestion and ESI-MS analysis of each collected peak are displayed. (C) CD spectra before (solid line) and after 10 min irradiation (dotted line) of a solution of $Zn\cdot L_{ASD}$(HHCC) (30 μM) containing rose bengal (3 μM), in 20 mM Pi (H_2O pH 7.0).

by ESI-MS analysis of the crude corresponds to the addition of two oxygen atoms to the peptide, suggesting the formation of sulfinates. Other peaks corresponding to the addition of three and four oxygen atoms are also observed. The two HPLC peaks were collected, digested with glutamate carboxypeptidase (GluC, a peptidase that cleaves peptides at carboxylic side of glutamates or aspartates), and digestion mixtures were analysed by ESI-MS (Fig. 5A and Table S1†). GluC digestion of L_{ASD}(HHCC) can give four fragments: Ac-KHVSKQLLKAYAE (F1), GTLSE (F2), AYSKK-VAKHLSKC^{31}E(E) (F3) and C^{34}KAKAQKLKAKAA-NH_2 (F4). Digestion of both HPLC fractions gave unaltered N-terminal fragments F1 and F2, meaning that neither His2 nor Tyr11 are photooxidized. However, different patterns were observed for the two cysteine-containing fragments F3 and F4 (Table S1 of ESI†). For both HPLC fractions, no mass peak corresponding to the possible F3–F4 disulfide was detected. For the fraction eluting at 20.3 min, fragment F3 is unaltered but fragment F4 was detected in three distinct chemical forms: unaltered and with increase of 32 and 48 mass units. The product with a 32 mass unit increase was ascribed to the oxidation of Cys34 into a sulfinate by comparison to previous studies.[21,22] This was confirmed by the loss of 66 mass units corresponding to H_2SO_2 upon MS/MS fragmentation. The formation of a sulfinate upon photooxidation of metal-bound thiolate has already been reported in many instances for Pt,[35–37] Ni,[38] Pd,[38] Co[39–41] and Cd[42] complexes thereby supporting the formation of a sulfinate for Zn-bond cysteines in $Zn\cdot L_{ASD}$(HHCC) but the product with a 48-mass unit increase is more intriguing. As F4 does not contain any amino acid prone to oxygen incorporation upon photooxidation other than Cys34 (*i.e.* His, Tyr, Trp or Met), this product could only be ascribed to the formation of a sulfonate on Cys34. This hypothesis is supported by the formation of glutathione sulfonate in the case of photooxidation of glutathione.[43] Nevertheless, the mechanism of the formation of this product, especially the breaking of the O–O bond in the putative $RS(O)(O)–OO^-$ intermediate remains

unclear. Altogether, the fraction eluting at 20.3 min contains the unoxidized peptide L_{ASD}(HHCC) as expected but also L_{ASD}(HHCC^{SO_2}) and L_{ASD}(HHCC^{SO_3}) oxidation products in which Cys34 was photooxidized into a sulfinate and a sulfonate, respectively (Fig. 5A). For the fraction eluting at 18.1 min, only a 32-mass unit increase was detected for F3, revealing photooxidation of Cys31 into a sulfinate (confirmed by loss of 66 mass units upon MS/MS fragmentation). Photooxidation of Cys31 rather than Tyr20 or His27 in F3 was supported by unaltered F1 fragment, which contains also histidine and tyrosine, and was further demonstrated by the loss of 66 Da corresponding to H_2SO_2 upon MS–MS fragmentation. F4 appears within three different forms: unaltered and with +32 and +48 mass units. This indicates the presence of Cys34 in reduced, sulfinate and sulfonate forms in the fraction eluting at 18.1 min. Therefore, this fraction contains three peptides: the primary oxidation product L_{ASD}(HHC^{SO_2}C) and the overoxidation products L_{ASD}(HHC^{SO_2}C^{SO_2}) and L_{ASD}(HHC^{SO_2}C^{SO_3}) (Fig. 5B). Noteworthy, mass analysis always revealed the presence of overoxidation products, even at short irradiation times, indicating that the rate of formation of overoxidation products is at least comparable to the rate of formation of primary oxidation products L_{ASD}(HHCC^{SO_2}) and L_{ASD}(HHC^{SO_2}C).

Then, the rate of chemical reaction between Zn·L_{ASD}(HHCC) and $^1O_2$ (k_r) was assessed by competitive photooxidation with the peptide EGWGK as a competitor (k_r(EGWGK) = (4.6 ± 0.5) × 10^6 M^{-1} s^{-1})[21] following a procedure described previously.[21,22] The method consists in comparing the consumption of the zinc finger peptide and the reference compound by HPLC (ESI). In such a competitive photooxidation experiment, the ratio of the rate constants k_{r1} and k_{r2} of two compounds C_1 and C_2 is given by eqn (1) where $[C_i]_0$ and $[C_i]_f$ are the concentrations of compound C_i before and after photooxidation, respectively.[44,45]

$$\frac{k_{r1}}{k_{r2}} = \frac{\ln\left([C_1]_f / [C_1]_0\right)}{\ln\left([C_2]_f / [C_2]_0\right)} \quad (1)$$

Since we were not able to separate unreacted L_{ASD}(HHCC) and L_{ASD}(HHCC^{SO_2}) by HPLC and as overoxidation are rapidly formed, this method underestimates the consumption of L_{ASD}(HHCC) and yields a sizeable underestimation of k_r. Nevertheless, a lower limit of 3.9 × 10^6 M^{-1} s^{-1} for k_r(Zn·L_{ASD}(HHCC)) was calculated from the competition experiments. Finally, CD was used to assess the consequences of $^1O_2$ oxidation of Zn·L_{ASD}(HHCC) on the peptide fold. As shown in Fig. 5C, photooxidation causes dramatic loss of helical structure, attesting of peptide unfolding.

Discussion

Design and characterization of the anti-sigma factor domain zinc finger model

For several years, we have been developing peptidic zinc finger models of small size in order to study the reactivity of zinc finger sites toward reactive oxygen species such as H_2O_2,[18–20] HOCl[34] or $^1O_2$ [21,22] at the molecular level. Our approach involves the use of cyclic and branched peptides, named CPLT (Cyclic Peptides with Linear Tail),[29] to create shortcuts in native zinc finger sequences. This affords models that reproduce almost perfectly the fold of native zinc finger domains around the Zn^{2+} ion with a minimal set of amino acids. The small size of these models allowed us to characterize oxidation products and to provide reliable kinetic data to describe the reactivity of zinc fingers. The CPLT design is well suited to zinc finger sites harbouring a CXXC motif in a β-hairpin loop. However, the elaboration of a CPLT model was not possible for the anti-sigma factor domain due to its 3-helix core that supports the four Zn^{2+}-binding amino acids. Therefore, we decided to keep this core but to reduce the size of the anti-sigma factor domain sequence as much as possible without altering its fold around Zn^{2+}. Re-engineering of the amino acid sequence allowed us to get a soluble 46-amino acid protein that folds upon Zn^{2+} binding and adopts the same conformation as that found in the sigma factor/anti-sigma factor complex. The design strategy used to elaborate this model revealed some important features: (i) it is necessary to avoid clustering of negatively or positively charged amino acids on the surface to provide sufficient solubility to the model, (ii) once the Zn^{2+} ion coordinated to the H–X_3–C–X_2–C motif, the constitution of a hydrophobic core within the heart of the 3-helix structure is most probably the driving force for the protein to get the proper folding; and (iii) the N-terminal histidine is absolutely required for conformational stability, providing at least 4 kcal mol^{-1} stabilization to the system as shown by the comparison between Zn·L_{ASD}(HHCC) and Zn·L_{ASD}(AHCC).

H_2O_2 and $^1O_2$ oxidation

In previous studies on the oxidation of model zinc fingers, we have shown that H_2O_2 yields mainly disulfides as products at physiological pH conditions whereas $^1O_2$ yields mainly sulfinates. Regarding kinetics, we have observed that neutral $Zn(Cys)_2(His)_2$ zinc finger sites react slower with H_2O_2 than negatively charged $Zn(Cys)_3(His)$ and $Zn(Cys)_4$ zinc finger sites.[19,20] The reactivity of Zn·L_{ASD}(HHCC) toward H_2O_2 was studied using the methodology previously described.[19] Reaction with H_2O_2 leads to disulfide formation within the CEEC motif with a second order rate constant of 0.030 ± 0.002 M^{-1} s^{-1} at 297 K. This is within the range of second order rate constants determined for other $Zn(Cys)_2(His)_2$ zinc fingers (k = 0.008–0.037 M^{-1} s^{-1}) but significantly lower than for $Zn(Cys)_3(His)$ and $Zn(Cys)_4$ zinc fingers (k = 0.1–1.5 M^{-1} s^{-1}), confirming the trend previously observed.[20] Among $Zn(Cys)_2(His)_2$ zinc fingers models, Zn·L_{ASD}(HHCC) reacts faster with H_2O_2 than Zn·CP-1(CCHH) (k = 0.008 M^{-1} s^{-1}), a classical CCHH zinc finger with well-defined ββα fold. Regarding $^1O_2$, reaction of Zn·L_{ASD}(HHCC) is very fast leading to sulfinates but overoxidation products (sulfonate, bis-sulfinate) are also formed very rapidly. No photooxidation of Zn^{2+}-bound histidines was detected, confirming that histidines are protected from $^1O_2$ oxidation by Zn^{2+} coordination, as previously observed in the case of a classical ββα zinc finger.[22] Unfortunately, all photooxidation products could not be separated by HPLC precluding precise determination of the chemical reaction rate constant k_r.[21,22] This was not the case in previous studies. Indeed, the size of the Zn·L_{ASD}(HHCC) model is large compared to our other

previously described models (46 *versus ca.* 25 amino acids), rendering HPLC separation less sensitive to changes occurring at a single amino acid position. Hence, the size of the model clearly matters for optimal separation and the smaller the model, the more detailed the molecular information. Nevertheless, a lower limit of 3.9×10^6 M^{-1} s^{-1} could be determined for k_r. The observation of at least two overoxidation products – even at short irradiation time – in the peak eluting at 20.3 min (Fig. 5A) during analysis of photooxidation products of Zn·L_{ASD}(HHCC) indicates that this k_r value is probably underestimated. Hence, Zn·L_{ASD}(HHCC) reacts with $^1O_2$ at least as fast as, but most probably faster than, Zn·L_{TC} ($k_r = (4.3 \pm 0.4) \times 10^6$ M^{-1} s^{-1}), a $Zn(Cys)_4$ treble clef zinc finger model, on contrary to what is observed for H_2O_2. In the case of H_2O_2, negatively charged $Zn(Cys)_4$ sites react faster than neutral $Zn(Cys)_2(His)_2$ sites. Therefore, the observed trend for H_2O_2 regarding the charge of the zinc finger site and its reactivity cannot be extrapolated to $^1O_2$ reactivity. The lower limit value of k_r determined for Zn·L_{ASD}(HHCC) is higher than the k_r value determined for Zn·CPF ($k_r = (0.70 \pm 0.07) \times 10^6$ M^{-1} s^{-1}), a model peptide for the CCHH classical ββα zinc fingers, which differs from Zn·CP-1(CCHH) by a single Tyr to Phe mutation only. In order to understand the greater reactivity of Zn·L_{ASD}(HHCC) compared to the classical ββα zinc finger CP-1/CPF observed for H_2O_2 and $^1O_2$, we have examined the structure of the $Zn(Cys)_2(His)_2$ sites in both models focusing on two important factors for cysteine sulfur reactivity: solvent accessible surface and number of NH···S hydrogen bonds, the latter being known to decrease the nucleophilic reactivity of Zn^{2+}-bound sulfurs.[23,46] Based on our NMR structure of Zn·L_{ASD}(HHCC) and the pdb file 1MEY[47] for Zn·CP-1(CCHH), we found that the former has higher sulfur solvent accessible surface area (8.8 $Å^2$ *vs.* 4.1 $Å^2$) and less NH···S hydrogen bonds (1 *vs.* 3). Therefore, these two factors support the greater reactivity of the anti-sigma factor domain zinc finger model compared to the classical ββα model.

Biological relevance

Zinc binding to ChrR and formation of the $Zn(Cys)_2(His)_2$ zinc finger site of ChrR is needed to ensure its proper folding and sequestering of σ^E.[8] Plus, it was demonstrated that the anti-sigma factor domain of ChrR is sufficient to sequester σ^E.[10] Our data show that the Zn·L_{ASD}(HHCC) model can be oxidized by $^1O_2$ leading to its unfolding. This supports the hypothesis that photooxidation of the cysteines of ChrR $Zn(Cys)_2(His)_2$ zinc finger site may be a key event in the $^1O_2$ sensing mechanism by ChrR promoting the breakdown the ChrR–σ^E complex. Nevertheless, to be a sensing unit this zinc finger site would require fast reaction with $^1O_2$ in order to trigger quickly the cellular response against $^1O_2$ before too many oxidative damages are produced. The kinetic data gained in this study are also in favour of a sensing role for ChrR $Zn(Cys)_2(His)_2$ site: it reacts with $^1O_2$ faster than other known structural zinc finger sites, either of the $Zn(Cys)_2(His)_2$ [22] or $Zn(Cys)_4$ [21] type. Indeed, it seems that the uncommon topology of the zinc finger site of ChrR[12] provides very high zinc affinity while maintaining "naked" cysteinates, with a low number of NH···S hydrogen bonds, for higher reactivity. However, Rajasekar *et al.* have shown that oxidation of the HHCC zinc finger of ZAS proteins is not always sufficient to dissociate the anti-sigma factor from its cognate sigma factor.[17] In the case of ChrR, it was clearly demonstrated that its C-terminal cupin-like domain is required for the $^1O_2$ response.[10,11,17] Therefore, it is possible that $^1O_2$ oxidation of both the zinc finger of ChrR anti-sigma factor domain and essential histidine residues of the cupin-like domain are required to cause sufficient conformational change to allow the dissociation of the ChrR–σ^E complex. This would correspond to a dual activation process making this system responsive to $^1O_2$ only among ROS, for a specific triggering of the transcriptional response. Alternatively, the essential histidine and glutamate residues of the cupin-like domain (H141, H143, E147 and H177) could provide alternative Zn^{2+} ligands to compensate for the oxidized cysteines of the anti-sigma factor domain. A mixed coordination set involving residues of both the anti-sigma factor domain and the cupin-like domain around Zn^{2+} would generate sufficient conformational rearrangement to destabilize the ChrR–σ^E complex.

Conclusions

In this article, we have described the elaboration of a model for the $Zn(Cys)_2(His)_2$ zinc finger site of the anti-sigma factor domain of ChrR, a protein involved in transcriptional response to $^1O_2$ in several bacteria. This site has a special topology among zinc fingers and its role in $^1O_2$ sensing by ChrR is under debate. This model, namely Zn·L_{ASD}(HHCC), is a 46-amino acid peptide inspired from ChrR anti-sigma factor domain sequence. It forms a 3-helix core when Zn^{2+} binds to the four cysteine and histidine side chains. Zn·L_{ASD}(HHCC) adopts the same structure as the corresponding sequence in ChrR anti-sigma factor domain. We have shown that the cysteines of the $Zn(Cys)_2(His)_2$ site of Zn·L_{ASD}(HHCC) are oxidized by $^1O_2$ into sulfinates and other overoxidation products. Photooxidation is faster than that of other zinc finger sites, especially compared to classical ββα $Zn(Cys)_2(His)_2$ zinc fingers. Additionally, $^1O_2$ oxidation destabilizes the zinc finger leading to its unfolding. The data presented in this work indicate that photooxidation of the zinc finger site of ChrR may be a key event in its $^1O_2$ sensing mechanism.

Conflicts of interest

There are no conflicts to declare.

Acknowledgements

This work has been partially supported by Labex ARCANE and CBH-EUR-GS (ANR-17-EURE-0003).

Notes and references

1 C. C. Winterbourn, in *Encyclopedia of Radicals in Chemistry, Biology and Materials*, John Wiley & Sons, Ltd, 2012.
2 C. S. Foote, *Photochem. Photobiol.*, 1991, **54**, 659.

3 E. C. Ziegelhoffer and T. J. Donohue, *Nat. Rev. Microbiol.*, 2009, **7**, 856–863.
4 M. S. Baptista, J. Cadet, P. Di Mascio, A. A. Ghogare, A. Greer, M. R. Hamblin, C. Lorente, S. C. Nunez, M. S. Ribeiro, A. H. Thomas, M. Vignoni and T. M. Yoshimura, *Photochem. Photobiol.*, 2017, **93**, 912–919.
5 B. B. Fischer, E. Hideg and A. Krieger-Liszkay, *Antioxid. Redox Signal.*, 2013, **18**, 2145–2162.
6 J. Glaeser, A. M. Nuss, B. A. Berghoff and G. Klug, in *Advances in Microbial Physiology*, ed. R. K. Poole, Academic Press Ltd, Elsevier Science Ltd, London, 2011, vol. 58, pp. 141–173.
7 L. O. Klotz, K. D. Kröncke and H. Sies, *Photochem. Photobiol. Sci.*, 2003, **2**, 88–94.
8 J. D. Newman, J. R. Anthony and T. J. Donohue, *J. Mol. Biol.*, 2001, **313**, 485–499.
9 J. R. Anthony, J. D. Newman and T. J. Donohue, *J. Mol. Biol.*, 2004, **341**, 345–360.
10 E. A. Campbell, R. Greenwell, J. R. Anthony, S. Wang, L. Lim, K. Das, H. J. Sofia, T. J. Donohue and S. A. Darst, *Mol. Cell*, 2007, **27**, 793–805.
11 R. Greenwell, T.-W. Nam and T. J. Donohue, *J. Mol. Biol.*, 2011, **407**, 477–491.
12 C. Andreini, I. Bertini and G. Cavallaro, *PLoS One*, 2011, **6**, e26325.
13 K. G. Thakur, T. Praveena and B. Gopal, *J. Mol. Biol.*, 2010, **397**, 1199–1208.
14 J. G. Kang, M. S. B. Paget, Y. J. Seok, M. Y. Hahn, J. B. Bae, J. S. Hahn, C. Kleanthous, M. J. Buttner and J. H. Roe, *EMBO J.*, 1999, **18**, 4292–4298.
15 K. Zdanowski, P. Doughty, P. Jakimowicz, L. O'Hara, M. J. Buttner, M. S. B. Paget and C. Kleanthous, *Biochemistry*, 2006, **45**, 8294–8300.
16 Y.-G. Jung, Y.-B. Cho, M.-S. Kim, J.-S. Yoo, S.-H. Hong and J.-H. Roe, *Nucleic Acids Res.*, 2011, **39**, 7586–7597.
17 K. V. Rajasekar, K. Zdanowski, J. Yan, J. T. S. Hopper, M.-L. R. Francis, C. Seepersad, C. Sharp, L. Pecqueur, J. M. Werner, C. V. Robinson, S. Mohammed, J. R. Potts and C. Kleanthous, *Nat. Commun.*, 2016, **7**, 12194.
18 O. Sénèque, E. Bourlès, V. Lebrun, E. Bonnet, P. Dumy and J.-M. Latour, *Angew. Chem., Int. Ed.*, 2008, **47**, 6888–6891.
19 E. Bourlès, M. Isaac, C. Lebrun, J.-M. Latour and O. Sénèque, *Chem.–Eur. J.*, 2011, **17**, 13762–13772.
20 M. Isaac, J.-M. Latour and O. Sénèque, *Chem. Sci.*, 2012, **3**, 3409–3420.
21 V. Lebrun, A. Tron, L. Scarpantonio, C. Lebrun, J.-L. Ravanat, J.-M. Latour, N. D. McClenaghan and O. Sénèque, *Angew. Chem., Int. Ed.*, 2014, **53**, 9365–9368.
22 V. Lebrun, A. Tron, C. Lebrun, J.-M. Latour, N. D. McClenaghan and O. Sénèque, *Chem.–Eur. J.*, 2015, **21**, 14002–14010.
23 A. T. Maynard and D. G. Covell, *J. Am. Chem. Soc.*, 2001, **123**, 1047–1058.
24 O. Sénèque and J.-M. Latour, *J. Am. Chem. Soc.*, 2010, **132**, 17760–17774.
25 V. Cornish, M. Kaplan, D. Veenstra, P. Kollman and P. Schultz, *Biochemistry*, 1994, **33**, 12022–12031.
26 J. Venkatraman, S. C. Shankaramma and P. Balaram, *Chem. Rev.*, 2001, **101**, 3131–3152.
27 *The PyMOL Molecular Graphics System*, Schrödinger, LLC, 2002.
28 P. White, J. W. Keyte, K. Bailey and G. Bloomberg, *J. Pept. Sci.*, 2004, **10**, 18–26.
29 A. Jacques, B. Mettra, V. Lebrun, J.-M. Latour and O. Sénèque, *Chem.–Eur. J.*, 2013, **19**, 3921–3931.
30 B. Krizek, D. Merkle and J. Berg, *Inorg. Chem.*, 1993, **32**, 937–940.
31 A. R. Reddi, T. R. Guzman, R. M. Breece, D. L. Tiemey and B. R. Gibney, *J. Am. Chem. Soc.*, 2007, **129**, 12815–12827.
32 D. A. Deranleau, *J. Am. Chem. Soc.*, 1969, **91**, 4044–4049.
33 D. A. Deranleau, *J. Am. Chem. Soc.*, 1969, **91**, 4050–4054.
34 V. Lebrun, J.-L. Ravanat, J.-M. Latour and O. Sénèque, *Chem. Sci.*, 2016, **7**, 5508–5516.
35 Y. Zhang, K. D. Ley and K. S. Schanze, *Inorg. Chem.*, 1996, **35**, 7102–7110.
36 W. B. Connick and H. B. Gray, *J. Am. Chem. Soc.*, 1997, **119**, 11620–11627.
37 D. Zhang, Y. Bin, L. Tallorin, F. Tse, B. Hernandez, E. V. Mathias, T. Stewart, R. Bau and M. Selke, *Inorg. Chem.*, 2013, **52**, 1676–1678.
38 C. A. Grapperhaus, M. J. Maguire, T. Tuntulani and M. Y. Darensbourg, *Inorg. Chem.*, 1997, **36**, 1860–1866.
39 C. Galvez, D. G. Ho, A. Azod and M. Selke, *J. Am. Chem. Soc.*, 2001, **123**, 3381–3382.
40 B. Hernandez, Y. J. Wang, D. Zhang and M. Selke, *Chem. Commun.*, 2006, 997–999.
41 D. Zhang, B. Hernandez and M. Selke, *J. Sulfur Chem.*, 2008, **29**, 377–388.
42 D. A. Cagan, A. C. Garcia, K. Li, D. Ashen-Garry, A. C. Tadle, D. Zhang, K. J. Nelms, Y. Liu, J. R. Shallenberger, J. J. Stapleton and M. Selke, *J. Am. Chem. Soc.*, 2019, **141**, 67–71.
43 T. Devasagayam and A. Sundquist, *J. Photochem. Photobiol., B*, 1991, **9**, 105–116.
44 R. Higgins, C. S. Foote and H. Cheng, *Adv. Chem. Ser.*, 1968, 102–117.
45 F. Wilkinson, W. Helman and A. Ross, *J. Phys. Chem. Ref. Data*, 1995, **24**, 663–1021.
46 Y.-M. Lee and C. Lim, *J. Am. Chem. Soc.*, 2011, **133**, 8691–8703.
47 C. A. Kim and J. M. Berg, *Nat. Struct. Biol.*, 1996, **3**, 940–945.

Model Peptide for Anti-Sigma Factor Domain HHCC Zinc Fingers: High Reactivity toward $^1O_2$ Leads to Domain Unfolding

Valentin Chabert,[a] Vincent Lebrun,[a] Colette Lebrun,[b] Jean-Marc Latour,[a] and Olivier Sénèque*[a]

[a] Univ. Grenoble Alpes, CNRS, CEA, BIG, LCBM (UMR 5249), F-38000 Grenoble, France.

[b] Univ. Grenoble Alpes, CEA, INAC, SyMMES, F-38000 Grenoble, France.

Email: *olivier.seneque@cea.fr*

Supporting Information

Content

Abbreviations

PyBOP: (Benzotriazol-1-yloxy)tripyrrolidino-phosphonium-hexafluorophosphate; $Pd(PPh_3)_4$: *tetrakis*(triphenyl-phosphine)-palladium(0); TIS: triisopropylsilane; TCEP: *tris*(2-carboxyethyl)phosphine; DIEA: N,N-diisopropylethylamine; TFA: trifluoroacetic acid; MeOH: methanol; DCM: dicholoromethane; Et_2O: diethylether; DMF: N,N-dimethylformamide; *t*Bu: *tert*-butyl; Trt: trityl; Fmoc: 9-fluorenylmethoxycarbonyl; Boc: *tert*-butyloxycarbobyl; EDTA: ethylenediamine-tetraacetic acid; HPLC: high performance liquid chromatography; ESI: electrospray ionization; MS: mass spectrometry; UV-Vis: ultraviolet-visible; CD: circular dichroism.

Materials and methods

Reagents and solvents: N-α-Fmoc-protected amino acids for peptide synthesis, PyBOP coupling reagent and NovaPEG Rink Amide resin were obtained from Novabiochem. Other reagents for peptide synthesis, solvents, buffers and metal salts were purchased from Sigma-Aldrich. All buffers or metal solutions were prepared with MilliQ water (Millipore). Buffer solutions were treated with Chelex 100 resin (Biorad) to remove trace metal ions. The concentration of the Zn^{2+} and Co^{2+} stock solutions was determined by colorimetric EDTA titrations.[1]

Analyses and purifications: RP-HPLC was used for analyses and purifications of the peptides. Mixtures of solvent A (0.1% TFA in H_2O) and B (0.1% TFA in MeOH/H_2O 9:1) were used as mobile phase. Analytical HPLC separations were performed on an Agilent Infinity 1200 system using Merck Chromolith RP-18e (150 mm × 4.6 mm) columns. Method A consisted in 5% B during 2 min, a 5 to 55 % B linear gradient in 5 min, then a 55 to 90 % B linear gradient in 15 min at 2 mL/min. Preparative HPLC separations were performed on a VWR LaPrepΣ system using a Waters XBridge Peptide BEH130 C18 (5 µm, 150 mm × 19 mm) column at 10 mL/min. The preparative separation method consisted in 5% B during 2 min, a 5 to 50 % B linear gradient in 5 min then a 50 to 90 % B linear gradient in 25 min at 10 mL/min. Eluate was monitored by electronic absorption at 214, 254 and 280. ESI-MS analyses were performed on a Thermo LXQ spectrometer. UV-Vis absorption spectra were recorded on a Perkin-Elmer Lambda 35 spectrophotometer or on a Varian Cary 50 spectrophotometer. Circular dichroism spectra were recorded on an Applied Photophysics Chirascan spectropolarimeter.

Peptide synthesis

Elongation of L_{ASD}(**X**HCC) Ac-K**X**VSKQLLKAYAEGTLSEAYSKKVAKHLSKCEECKAKAQKLKAKAA-NH_2 (with **X** = H or A) was performed on NovaPEG Rink Amide resin (0.40 mol g^{-1}; 0.13 mmol scale) using standard SPPS protocols using Fmoc/tBu chemistry on an automated peptide synthesizer (CEM Liberty1 Microwave Peptide Synthesizer) after attachment of the first amino acid by single manual coupling (30 min) using 2-fold excess of Fmoc-Gly-OH, 2-fold excess of PyBOP and 6-fold excess of DIEA in DMF followed by acetylation using Ac_2O/pyridine/DMF (1:2:7 (by vol.), 10 mL, 5 min). For automated synthesis, single coupling (5 min, 50°C, 25 W microwave power) were performed using 4-fold molar excess of Fmoc-L-amino acid, 4-fold molar excess of PyBOP and 8-fold molar excess of DIEA. A capping step was performed after each coupling with Ac_2O/DIEA in DMF (5 min, 65 °C, 40 W microwave power). Fmoc removal was performed using 20% piperidine in DMF (30 s + 3 min, 70°C, 40 W microwave power). Dipeptides underlined in the above sequence were introduced as pseudo-proline dipeptides (Fmoc-Val-Ser($\Psi^{Me,Me}$pro)-OH, Fmoc-Gly-Thr($\Psi^{Me,Me}$pro)-OH, Fmoc-Tyr(*t*Bu)-Ser($\Psi^{Me,Me}$pro)-OH and Fmoc-Leu-Ser($\Psi^{Me,Me}$pro)-OH) by manual coupling as describe above for the

first amino acid. Before the last two amino acids, the resin was divided into two parts in a 6:1 ratio. The KA terminus was assembled on the small batch and the KH terminus on the biggest. The N-terminus was acetylated manually using Ac_2O/pyridine/DMF (1:2:7 (by vol.), 10 mL, 5 min). Removal of acid-labile protecting groups and resin cleavage were performed using TFA/H_2O/TIS/DTT (19 mL:0.6 mL:0.6 mL:600 mg) for 2 h. TFA was evaporated under reduced pressure and cold Et_2O was added to precipitate the peptide. The pure peptide was obtained after HPLC purification and freeze-drying. **L_{ASD}(HHCC):** Yield = 13 % (98 mg); HPLC (anal.) t_R = 14.7 min (method A); ESI-MS: average *m/z* = 1272.7 (4+), 1018.3 (5+), 848.8 (6+), 727.8 (7+), 636.9 (8+), 566.3 (9+), 509.8 (10+) / calculated av. *m/z* = 1272.75 $[M+4H]^{4+}$, 1018.40 $[M+5H]^{5+}$, 848.84 $[M+6H]^{6+}$, 727.72 $[M+7H]^{7+}$, 636.88 $[M+8H]^{8+}$, 566.23 $[M+9H]^{9+}$, 509.71 $[M+10H]^{10+}$ for M = $C_{225}H_{383}N_{65}O_{64}S_2$). **$L_{ASD}$(AHCC):** Yield = 13 % (16 mg); HPLC (anal.) t_R = 16.6 min (method A); ESI-MS: average *m/z* = 1256.1 (4+), 1005.0 (5+), 837.7 (6+), 718.3 (7+), 628.7 (8+), 558.9 (9+) / calculated av. *m/z* = 1256.24 $[M+4H]^{4+}$, 1005.19 $[M+5H]^{5+}$, 837.83 $[M+6H]^{6+}$, 718.28 $[M+7H]^{7+}$, 628.62 $[M+8H]^{8+}$, 558.89 $[M+9H]^{9+}$ for M = $C_{222}H_{381}N_{63}O_{64}S_2$).

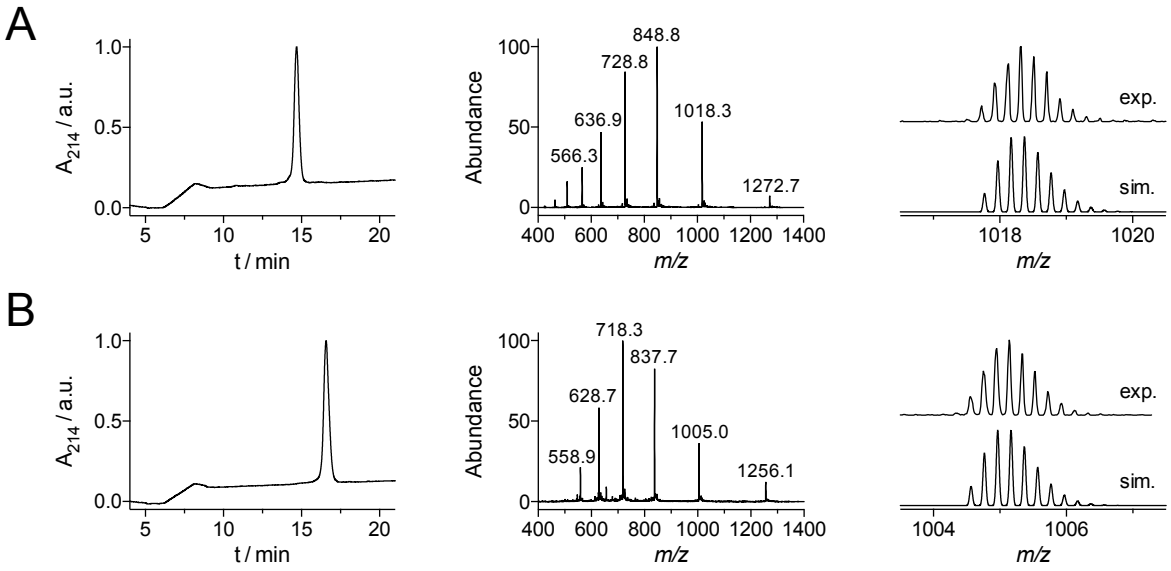

Fig. S1 HPLC chromatograms (*left*) and ESI-MS spectra (*middle*: full MS spectrum; *right*: experimental and simulated isotopic pattern of the $[M+5H]^{5+}$ peak) of (A) L_{ASD}(HHCC) and (B) L_{ASD}(AHCC).

Preparation of zinc finger stock solutions

Solutions of metal-free L_{ASD} peptides (*ca.* 1 mM) were prepared by dissolution of the lyophilized peptides in H_2O (or D_2O for photooxidation experiments) under argon atmosphere. The exact peptide concentration was determined by Ellman's assay.[2] Solutions of Zn·L_{ASD} (*ca.* 1 mM) complexes were prepared by adding 1.1 eq. of Zn^{2+} dissolved H_2O (100 mM). The pH was adjusted to 7.0 using NaOH (or NaOD).

Absorption and circular dichroism

A solution of metal-free L_{ASD} peptide (10-20 µM and 100-150 µM for Zn^{2+} and Co^{2+} titrations, respectively) in phosphate buffer (20 mM, pH 7.0) containing TCEP (250 µM) was prepared from stock solutions of peptide, phosphate buffer (100 mM, pH 7.0) and TCEP (33 mM). Titrations were performed at 298 K under argon by adding aliquots of a degassed metal stock solution to a rubber-sealed quartz cell (0.4 cm or 1 cm path length) containing the peptide solution. UV-Vis spectra were recorded every 1 nm at a scan rate of 240 nm/min. CD

spectra were recorded from 300 nm to 200 nm every 1 nm with a 2 s signal averaging for each point. Each spectrum was recorded twice, averaged and smoothed using a Savitzky-Golay filter.

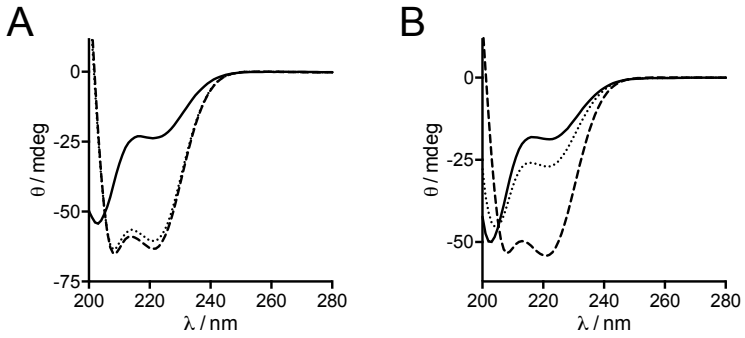

Fig. S2 Assessment of Zn^{2+} binding constants by competition experiments. CD spectra of solutions containing L_{ASD}(HHCC) (A) or L_{ASD}(AHCC) (B) and one equivalent of EDTA in phosphate buffer (10 mM, pH 7.0) before addition of Zn^{2+} (solid lines) and after addition of 1.0 eq. Zn^{2+} (dotted lines) and 2.0 eq. Zn^{2+} (dashed lines).

Oxidation by H_2O_2

A solution of Zn·L_{ASD}(HHCC) (20 μM) and H_2O_2 (5-35 mM) was prepared in an appropriate buffer (pH 7.0) and the reaction was monitored by absorption spectrophotometry. Based on previous work, the decay of the LMCT band at 220 nm was used to monitor the reaction in phosphate buffer (100 mM).[3] The kinetic traces (Fig. S3A) could be fitted by mono-exponential to yield the apparent first-order rate constants, k^{obs}. Fig. S3B shows the linear dependence of k^{obs} against [H_2O_2], which yielded k = 0.031 ± 0.003 M^{-1} s^{-1}. Fig. S3C shows the CD spectra recorded before introduction of H_2O_2 (1 mM) and after reaction (15 h). The PAR assay was thus used to confirm the value of k.[3] Oxidations were conducted in presence of PAR (100 μM) in Bis-Tris buffer 1(00 mM) and the appearance of $Zn(PAR)_2$ absorption at 494 nm was recorded. Mono-exponential fit of the kinetic traces yielded k^{obs} values, which were plotted against [H_2O_2] to yield k = 0.030 ± 0.001 M^{-1} s^{-1} (Fig. S3D).

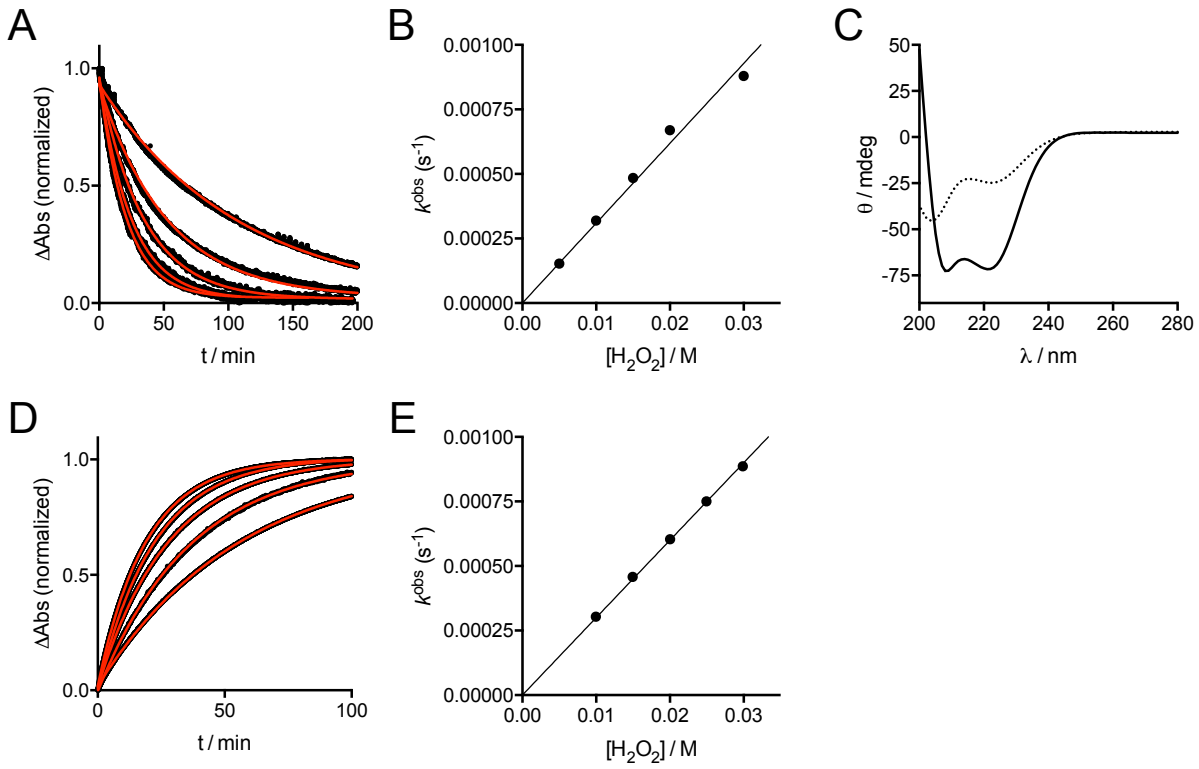

Fig. S3 Oxidation of Zn·L_{ASD}(HHCC) by H_2O_2. (A) Kinetic traces (black, normalized) for the LMCT monitoring (220 nm) with mono-exponential fits in red. (B) Plot of k^{obs} against $[H_2O_2]$ for the LMCT monitoring. The solid line corresponds to the linear regression yielding $k = 0.031 \pm 0.003$ M^{-1} s^{-1}. (C) CD spectra recorded before (solid line) and after (dashed line) reaction with H_2O_2. (D) Kinetic traces (black, normalized) for the PAR monitoring (494 nm) with mono-exponential fits in red. (E) Plot of k^{obs} against $[H_2O_2]$ for the PAR monitoring. The solid line corresponds to the linear regression yielding $k = 0.029 \pm 0.001$ M^{-1} s^{-1}.

Oxidation by $^1O_2$

Buffers: Deuterated buffer solutions were prepared by dissolving Na_2HPO_4 or ammonium acetate in D_2O (99,9% from Eurisotop, traces of metals removed by passing D_2O over CHELEX resin), and the pD was adjusted to 7.0 or 8.0 (with a regular pH meter, pD = pH_{red} + 0.44)[4] with NaOD and DCl. Otherwise, buffer solutions were prepared in milliQ H_2O.

Photooxidation: Typical photooxidation experiments were performed as follows. In an Eppendorf tube, the solution of Zn·L_{ASD}(HHCC) in D_2O is diluted to 200 µM in buffer Pi 20 mM pD containing 1-3 µM photosensitizer (Rose Bengal or Methylene Blue). The sample is maintained at 278 K in a water-cooled bath in front of a 400 W halogen lamp. After *ca.* 5 min of temperature equilibration, irradiation is performed by turning the lamp on for 30 seconds to 10 minutes, depending on the sample and solvent (shorter irradiation times are required for D_2O solution compared to H_2O). Then, the sample (100-300 µL) is injected into the HPLC for analysis. CD monitoring of the photooxidation was performed using H_2O solutions.

Determination of the lower limit for the photo-oxidation rate k_r of Zn·L_{ASD}(HHCC): The competition experiments were conducted as previously described[5,6] using peptide EGWGK as a competitor. Photooxidation was performed following the photooxidation protocol described above, but in presence of methylene blue as photosensitizer and in 20 mM Pi pD 8.0. Consumption of the two competitors was monitored by integration of the

HPLC chromatograms obtained before and after irradiation. As noted in the text, the peak eluting at 20.3 min contains unreacted L_{ASD}(HHCC) as well as some oxidized peptides, but we considered that it contains L_{ASD}(HHCC) only. This led to underestimate the consumption of L_{ASD}(HHCC). The chemical reaction rate constant was calculated using the equation given in the article. Therefore, only a lower limit of k_r was obtained: $k_r(Zn{\cdot}L_{ASD}(HHCC)) < (3.9 \pm 0.5)\times10^6\ M^{-1}\ s^{-1}$.

ESI-MS analysis of photooxidation products: For ESI-MS analysis of the reaction mixture, Zn·L_{ASD}(HHCC) was photooxidized in ammonium acetate buffer (20 mM in D_2O, pD 7.0) and the solution was lyophilized. The resulting solid was dissolved in H_2O containing 0.1 % TFA and lyophilized three times for complete D/H exchange before ESI-MS analysis. Finally, the solid was dissolved in ammonium acetate (20 mM, pH 7.0) and analyzed by ESI-MS. For digestion experiments, products were separated by HPLC, collected and lyophilized. The two collected fractions (0.1-0.2 mg) were dissolved in ammonium acetate (20 mM, pH 7.0, 190 µL). Glutamate carboxypeptidase GluC (200 ng×µL^{-1}, 10 µL) was added and solutions were incubated overnight at 37°C before freeze-drying. Fractions were dissolved in 0.1% TFA in H_2O or ammonium acetate (with or without TCEP) and analyzed by ESI-MS.

Table S1 ESI-MS analysis of GluC digested HPLC fractions of the photooxidation products of Zn·L_{ASD}(HHCC).

Fragment	Mass / Da	Observed *m/z* / Da for $[M+nH]^{n+}$ or $[M-nH]^{n-}$ species	
		peak eluting at 18.1 min	peak eluting at 20.3 min
Ac-KHVSKQLLKAYAE			
unaltered	1555.87	1556.8 (1+), 779.3 (2+), 519.8 (3+), 1554.6 (1–), 776.8 (2–), 1668.8 (1–) ($M+CF_3COO^-$)	1556.8 (1+), 779.6 (2+) 1554.6 (1–)
AYSKKVAKHLSKC$_{31}$EE			
unaltered (CysSH)	1719.90	–	861.1 (2+), 1718.8 (1–)
sulfinic acid ($CysSO_2H$)	1751.89	877.2 (2+), 585.3 (3+) 1750.8 (1–)*, 874.8 (2–), 931.6 (2–) ($M+CF_3COO^-$)	–
C_{34}KAKAQKLKAKAA-NH_2			
unaltered (CysSH)	1356.85	1357.6 (1+), 679.3 (2+) 1469.2 (1–) ($M+CF_3COO^-$)	1357.8 (1+), 679.6 (2+) 1355.7 (1–)
sulfinic acid ($CysSO_2H$)	1388.83	1387.6 (1–)*	1387.5 (1–)
sulfonic acid ($CysSO_3H$)	1404.82	1403.5 (1–)	1403.6 (1–)

* loss of 66 mass units (H_2SO_2) in MS/MS fragmentation.

Solution structure determination

NMR spectroscopy: All NMR experiments were recorded on a 500 MHz Bruker AVANCE II spectrometer equipped with a BBI probe with a z-axis gradient field. Samples were prepared by adding 1.1 molar equivalent of $Zn(ClO_4)_2$ to the peptide (*ca.* 1.8 mM) in H_2O/D_2O 9:1. The pH was adjusted to 6.3 with NaOH and HCl. 1D ^1H NMR spectra were recorded with 12-ppm window and 32k data points in the time domain. 2D ^1H-^1H spectra were acquired with Watergate[7,8] solvent suppression in phase-sensitive mode using 4096×1024 matrices over a 5000 Hz spectral width. TOCSY experiments were recorded at 298 K and 283 K using a MLEV-17 spin-lock sequence with a 70 ms mixing time. NOESY experiments were recorded at 298 K with a 200 ms mixing time. DQF-COSY spectra were recorded at 298 K. All spectra were processed with TOPSPIN 3.2.

Structure calculations: Cross peaks in NOESY spectra were integrated using the program SPARKY 3.114[9] and converted to H-H distances. Tyr Hδ/Hε (2.44 Å), Leu Hγ/Hδ, Thr Hβ/Hγ, Val Hβ/Hγ (2.80 Å) and His Hε1/Hδ2 (4.21 Å) were used as references for distance calibrations. Multiplicity was taken into account. Upper distance restraints were set to 2.7 Å, 3.5 Å, 5.0 Å and 7.0 Å for distances ≤ 2.5 Å, ≤ 3.3 Å, ≤ 4.8 Å and ≥ 4.8 Å, respectively. $^3J_{HN,H\alpha}$ coupling constants were measured on 1D ^{1}H NMR spectra experiments. ϕ dihedral restraints were derived from $^3J_{HN,H\alpha}$. Non-stereospecifically assigned protons were treated as pseudo-atoms. All peptide bond ω angles were set to *trans*. Solution structures were calculated using the program X-PLOR 3.851[10] following standard refinement protocols starting from random structures with r^{-6} averaging. The non-bonded interactions were modeled by the PARALLHDG force field. A first calculation was performed not including the zinc ion in the topology file to determine the overall fold of the peptide. The structure revealed the folding of helix H1, H2 and H3 and their close packing. The side chains of the two His and the two Cys residues were also very close, indicating their binding to the zinc ion. This calculation ensured that introducing a tetrahedral $Zn(Cys)_2(His)_2$ core in the topology file would not bias the structure. It also allowed determining which His N was bound to zinc. In house modifications were thus incorporated in the topology and parameter files (topallhdg.pro and parallhdg.pro) to account for for zinc binding to cysteines and histidines in a tetrahedral geometry with 2.33 Å and 2.00 Zn-S and Zn-N bonds, respectively, 109.4°, 109.4°, 105° and 125° S-Zn-S and S-Zn-N, Zn-S-C and Zn-N-C angles, respectively. Structures selected for analysis had no NOE violations greater than 0.2 Å and no dihedral angle violations greater than 5°.

Fig. S4 Summary of ^{1}H NMR data for Zn·L$_{ASD}$(HHCC) in H_2O/D_2O 9:1 (pH 6.4) at 298 K.

Table S2 ^{1}H NMR (500 MHz) coupling constants ($^3J_{HN,H\alpha}$ / Hz) and chemical shifts (δ / ppm) for Zn·L$_{ASD}$(HHCC) in H_2O/D_2O 9:1 (pH 6.4) at 298 K.[a]

Residue	$^3J_{HN,H\alpha}$	δ(HN)	δ(Hα)	δ(Hβ)	δ(others)
Ac	–	–	2.018		
LYS 1	n.d.	8.040	4.100	1.576, 1.649	CH_2(γ): 1.340; CH_2(δ): 1.357; CH_2(ε): 3.008
HIS 2	n.d.	7.830	4.300	2.797, 2.902	
VAL 3	7.0	6.930	3.960	1.983	CH_3(γ): 1.065, 1.148
SER 4	< 4	8.172	4.353	4.095	
LYS 5	4.2	8.867	3.936	1.871, 1.972	CH_2(γ): 1.521; CH_2(δ): 1.752; CH_2(ε): 3.024
GLN 6	4.0	8.556	4.032	2.004, 2.111	CH_2(γ): 2.477; NH(ε): 6.908, 7.552
LEU 7	7.9	7.623	4.200	1.294, 1.908	CH_2(γ): 1.562; CH_3(δ): 0.736, 0.898
LEU 8	< 5	8.484	4.026	1.412, 1.875	CH_2(γ): 1.736; CH_3(δ): 0.873, 0.942

LYS 9	4.1	8.109	3.967	1.880, 1.937	$CH_2(\gamma)$: 1.358, 1.481; $CH_2(\delta)$: 1.700; $CH_2(\varepsilon)$: 3.036
ALA 10	< 4	7.528	4.194	1.445	
TYR 11	2.5	8.791	4.175	3.192, 3.387	CH(δ): 6.989; CH(ε): 6.866
ALA 12	3.7	8.608	3.893	1.574	
GLU 13	7.9	8.190	4.183	2.088, 2.157	$CH_2(\gamma)$: 2.328, 2.599
GLY 14	–	7.819	3.979, 4.100		
THR 15	9.7	8.264	4.440	4.541	$CH_3(\gamma)$: 1.117
LEU 16	7.2	7.417	4.545	1.752	$CH_2(\gamma)$: 1.747; $CH_3(\delta)$: 0.965, 1.085
SER 17	3.7	8.598	4.486	4.167, 4.368	
GLU 18	2.7	9.130	4.157	2.094, 2.183	$CH_2(\gamma)$: 2.302, 2.416
ALA 19	2.8	8.572	4.106	1.350	
TYR 20	7.4	7.696	4.423	3.089	CH(δ): 7.211; CH(ε): 6.899
SER 21	3.1	9.094	4.229	4.144	
LYS 22	3.7	8.169	4.155	1.953	$CH_2(\gamma)$: 1.519; $CH_2(\delta)$: 1.736; $CH_2(\varepsilon)$: 3.025
LYS 23	5.4	7.335	4.064	1.983	$CH_2(\gamma)$: 1.424; $CH_2(\delta)$: 1.624; $CH_2(\varepsilon)$: 2.896
VAL 24	4.3	8.278	3.480	1.992	$CH_3(\gamma)$: 0.355, 1.040
ALA 25	2.5	8.666	3.776	1.639	
LYS 26	5.0	7.866	4.103	1.978	$CH_2(\gamma)$: 1.544; $CH_2(\delta)$: 1.725; $CH_2(\varepsilon)$: 3.009
HIS 27	5.9	7.675	4.321	3.230, 3.284	CH(δ), 6.893; CH(ε): 7.833
LEU 28	3.1	8.526	3.854	1.396, 1.799	$CH_2(\gamma)$: 1.767; $CH_3(\delta)$: 0.636
SER 29	< 5	7.612	4.198	4.029	
LYS 30	9.9	7.073	4.628	1.711, 1.950	$CH_2(\gamma)$: 1.362; $CH_2(\delta)$: 1.610; $CH_2(\varepsilon)$: 2.860
CYS 31	9.1	7.525	4.643	1.858, 2.519	
GLU 32	3.7	8.993	4.087	2.075, 2.165	$CH_2(\gamma)$: 2.385, 2.453
GLU 33	n.d.	8.381	4.191	1.936	$CH_2(\gamma)$: 2.242
CYS 34	5.6	9.284	4.117	2.868, 3.135	
LYS 35	< 6	8.378	3.867	1.926, 2.231	$CH_2(\gamma)$: 1.569; $CH_2(\delta)$: 1.412; $CH_2(\varepsilon)$: 2.949
ALA 36	4.1	8.140	4.249	1.575	
LYS 37	< 6	7.608	4.010	1.872, 2.025	$CH_2(\gamma)$: 1.434; $CH_2(\delta)$: 1.745; $CH_2(\varepsilon)$: 2.928
ALA 38	< 6	8.487	4.047	1.649	
GLN 39	n.d.	8.240	4.071	2.198, 2.302	$CH_2(\gamma)$: 2.508, 2.636; NH(ε): 6.931, 7.467
LYS 40	5.3	7.769	4.174	1.991	$CH_2(\gamma)$: 1.523; $CH_2(\delta)$: 1.690; $CH_2(\varepsilon)$: 3.015
LEU 41	< 6	7.849	4.169	1.493	$CH_2(\gamma)$: 1.888; $CH_3(\delta)$: 0.862, 0.911
LYS 42	5.8	7.961	4.249	1.909	$CH_2(\gamma)$: 1.572; $CH_2(\delta)$: 1.728; $CH_2(\varepsilon)$: 3.033
ALA 43	5.6	7.998	4.310	1.472	
LYS 44	< 6	8.025	4.085	1.915, 1.990	$CH_2(\gamma)$: 1.591; $CH_2(\delta)$: 1.738; $CH_2(\varepsilon)$: 3.007
ALA 45	5.0	7.935	4.276	1.509	
ALA 46	> 6	8.045	4.284	1.469	

[a] Chemical shifts are measured relative to external DSS.

Table S3 NOE-derived distances (Å) used for calculations with X-PLOR for Zn·L_{ASD}(HHCC).

LYS	1	HN	LYS	1	HA	3.35	LYS	22	HN	LYS	22	HD*	2.90
LYS	1	HN	HIS	2	HN	3.48	LYS	22	HN	LYS	23	HN	2.74
HIS	2	HD2	LYS	1	HA	3.99	LYS	23	HB*	TYR	20	HA	2.98
HIS	2	HD2	LYS	1	HB*	4.24	LYS	23	HN	TYR	20	HA	3.13
HIS	2	HN	LYS	1	HA	2.31	LYS	23	HN	SER	21	HA	4.03
HIS	2	HB*	HIS	2	HA	2.73	LYS	23	HN	LYS	22	HA	3.27
HIS	2	HD2	HIS	2	HA	3.91	LYS	23	HN	LYS	22	HB*	3.41
HIS	2	HD2	HIS	2	HB*	2.86	LYS	23	HN	LYS	23	HA	2.74
HIS	2	HE1	HIS	2	HN	3.37	LYS	23	HN	LYS	23	HB*	2.57
HIS	2	HN	HIS	2	HA	3.70	LYS	23	HN	LYS	23	HD*	3.67
HIS	2	HN	HIS	2	HB*	2.78	LYS	23	HN	LYS	23	HG*	4.02
HIS	2	HN	HIS	2	HD2	3.39	LYS	23	HN	VAL	24	HG*	5.14
HIS	2	HN	VAL	3	HN	3.57	VAL	24	HG*	VAL	3	HG*	5.42
VAL	3	HG*	HIS	2	HA	4.72	VAL	24	HG*	LEU	8	HA	4.53
VAL	3	HG*	HIS	2	HB*	4.97	VAL	24	HG*	LEU	8	HD*	4.89
VAL	3	HN	HIS	2	HA	2.48	VAL	24	HG*	TYR	11	HA	4.18

VAL	3	HN	HIS	2	HB*	2.63
VAL	3	HG*	VAL	3	HA	3.30
VAL	3	HN	VAL	3	HA	2.94
VAL	3	HN	VAL	3	HB	2.60
VAL	3	HN	VAL	3	HG*	3.40
VAL	3	HG*	LEU	7	HB*	4.05
VAL	3	HG*	LEU	8	HA	4.64
VAL	3	HG*	LEU	8	HG	4.09
VAL	3	HG*	VAL	24	HA	3.67
VAL	3	HG*	HIS	27	HB*	4.14
SER	4	HN	VAL	3	HA	2.23
SER	4	HN	VAL	3	HG*	3.67
SER	4	HN	SER	4	HA	2.63
SER	4	HN	SER	4	HB*	2.50
SER	4	HN	LEU	7	HD*	5.79
SER	4	HN	LEU	7	HN	3.54
SER	4	HN	LEU	8	HD*	4.27
LYS	5	HN	SER	4	HA	2.51
LYS	5	HN	SER	4	HB*	3.88
LYS	5	HN	SER	4	HN	4.28
LYS	5	HN	LYS	5	HA	3.07
LYS	5	HN	LYS	5	HB*	3.03
LYS	5	HN	LYS	5	HG*	4.03
LYS	5	HN	GLN	6	HN	3.39
GLN	6	HN	SER	4	HA	3.58
GLN	6	HN	LYS	5	HA	3.45
GLN	6	HN	LYS	5	HB*	2.93
GLN	6	HN	GLN	6	HA	2.77
GLN	6	HN	GLN	6	HB*	2.84
GLN	6	HN	GLN	6	HG*	3.71
GLN	6	HN	LEU	7	HN	2.77
LEU	7	HN	VAL	3	HG*	4.96
LEU	7	HD*	SER	4	HA	4.65
LEU	7	HN	GLN	6	HB*	2.95
LEU	7	HB*	LEU	7	HA	2.81
LEU	7	HD*	LEU	7	HA	3.45
LEU	7	HN	LEU	7	HA	3.08
LEU	7	HN	LEU	7	HB*	2.66
LEU	7	HN	LEU	7	HD*	4.21
LEU	7	HN	LEU	7	HG	3.31
LEU	7	HD*	TYR	20	HB*	5.56
LEU	8	HN	VAL	3	HG*	4.13
LEU	8	HD*	LYS	5	HA	3.92
LEU	8	HN	LYS	5	HA	3.07
LEU	8	HN	LEU	7	HA	3.26
LEU	8	HN	LEU	7	HB*	3.60
LEU	8	HN	LEU	7	HG	3.34
LEU	8	HN	LEU	7	HN	2.42
LEU	8	HD*	LEU	8	HA	3.09
LEU	8	HN	LEU	8	HB*	2.69
LEU	8	HN	LEU	8	HD*	3.63
LEU	8	HN	LEU	8	HG	2.55
LEU	8	HN	LYS	9	HN	2.65
LEU	8	HN	ALA	10	HN	3.74
LEU	8	HD*	CYS	34	HB*	4.59
LYS	9	HN	LEU	7	HN	3.40
LYS	9	HN	LEU	8	HA	2.93
LYS	9	HN	LEU	8	HD*	5.09
LYS	9	HN	LYS	9	HA	2.64
LYS	9	HN	LYS	9	HB*	2.37
VAL	24	HG*	TYR	11	HB*	3.71
VAL	24	HG*	LEU	16	HB*	4.24
VAL	24	HG*	TYR	20	HA	5.37
VAL	24	HG*	SER	21	HA	4.15
VAL	24	HN	SER	21	HA	3.14
VAL	24	HN	LYS	23	HA	2.80
VAL	24	HN	LYS	23	HN	2.61
VAL	24	HB	VAL	24	HA	2.83
VAL	24	HG*	VAL	24	HA	3.06
VAL	24	HN	VAL	24	HA	2.82
VAL	24	HN	VAL	24	HB	2.22
VAL	24	HN	VAL	24	HG*	3.23
VAL	24	HG*	ALA	25	HA	4.70
VAL	24	HG*	ALA	25	HB*	4.69
VAL	24	HN	ALA	25	HB*	3.68
VAL	24	HG*	LEU	28	HD*	4.04
ALA	25	HN	TYR	11	HD*	4.48
ALA	25	HN	TYR	11	HE*	3.90
ALA	25	HN	SER	21	HA	3.70
ALA	25	HB*	LYS	22	HA	3.01
ALA	25	HN	LYS	22	HA	3.16
ALA	25	HN	LYS	23	HA	4.16
ALA	25	HN	LYS	23	HN	3.89
ALA	25	HN	VAL	24	HA	3.39
ALA	25	HN	VAL	24	HB	2.56
ALA	25	HN	VAL	24	HG*	3.92
ALA	25	HN	VAL	24	HN	2.69
ALA	25	HN	ALA	25	HA	2.79
ALA	25	HN	ALA	25	HB*	2.87
ALA	25	HN	LYS	26	HN	2.79
ALA	25	HN	HIS	27	HN	4.13
ALA	25	HN	LEU	28	HD*	5.45
LYS	26	HN	ALA	25	HA	3.37
LYS	26	HN	ALA	25	HB*	3.16
LYS	26	HN	LYS	26	HA	2.85
LYS	26	HN	LYS	26	HB*	2.43
LYS	26	HN	HIS	27	HN	2.69
HIS	27	HD2	HIS	2	HA	3.09
HIS	27	HE1	HIS	2	HA	2.72
HIS	27	HD2	VAL	3	HA	3.82
HIS	27	HD2	VAL	3	HB	3.35
HIS	27	HD2	VAL	3	HG*	3.49
HIS	27	HE1	VAL	3	HG*	6.12
HIS	27	HN	VAL	3	HG*	4.87
HIS	27	HD2	LEU	8	HD*	5.08
HIS	27	HD2	VAL	24	HA	4.31
HIS	27	HD2	VAL	24	HG*	5.62
HIS	27	HN	VAL	24	HA	3.25
HIS	27	HN	VAL	24	HG*	5.68
HIS	27	HN	LYS	26	HB*	2.93
HIS	27	HB*	HIS	27	HA	2.69
HIS	27	HD2	HIS	27	HB*	3.07
HIS	27	HN	HIS	27	HA	2.85
HIS	27	HN	HIS	27	HB*	2.59
HIS	27	HD2	LEU	28	HA	3.47
HIS	27	HD2	LEU	28	HD*	3.69
HIS	27	HD2	LEU	28	HG	3.94
HIS	27	HN	LEU	28	HD*	5.17
HIS	27	HD2	CYS	31	HB*	3.35
HIS	27	HE1	CYS	31	HB*	3.48

LYS	9	HN	ALA	10	HN	2.72
LYS	9	HN	LEU	41	HD*	4.09
ALA	10	HN	GLN	6	HA	3.33
ALA	10	HN	LYS	9	HA	3.30
ALA	10	HN	LYS	9	HB*	2.89
ALA	10	HN	ALA	10	HA	2.54
ALA	10	HN	ALA	10	HB*	2.40
ALA	10	HB*	LEU	16	HA	4.05
ALA	10	HN	LEU	16	HD*	4.88
TYR	11	HE*	VAL	3	HG*	4.92
TYR	11	HB*	LEU	8	HA	2.76
TYR	11	HD*	LEU	8	HA	3.64
TYR	11	HD*	LEU	8	HD*	5.57
TYR	11	HN	LEU	8	HA	3.15
TYR	11	HN	LYS	9	HA	3.98
TYR	11	HN	LYS	9	HN	4.00
TYR	11	HN	ALA	10	HA	3.08
TYR	11	HN	ALA	10	HB*	3.40
TYR	11	HN	ALA	10	HN	2.74
TYR	11	HB*	TYR	11	HA	2.62
TYR	11	HD*	TYR	11	HA	2.76
TYR	11	HD*	TYR	11	HB*	2.78
TYR	11	HE*	TYR	11	HB*	3.63
TYR	11	HN	TYR	11	HA	2.77
TYR	11	HN	TYR	11	HB*	2.49
TYR	11	HN	TYR	11	HD*	3.76
TYR	11	HD*	ALA	12	HA	3.56
TYR	11	HD*	ALA	12	HB*	4.44
TYR	11	HE*	ALA	12	HA	4.12
TYR	11	HE*	ALA	12	HB*	5.21
TYR	11	HN	ALA	12	HB*	4.65
TYR	11	HN	ALA	12	HN	2.73
TYR	11	HN	GLU	13	HN	4.08
TYR	11	HD*	LEU	16	HD*	3.96
TYR	11	HD*	LEU	16	HG	3.59
TYR	11	HE*	LEU	16	HD*	5.73
TYR	11	HN	LEU	16	HD*	3.99
TYR	11	HN	LEU	16	HG	3.42
TYR	11	HD*	SER	21	HA	3.02
TYR	11	HE*	SER	21	HA	3.51
TYR	11	HE*	SER	21	HB*	3.45
TYR	11	HD*	VAL	24	HB	3.22
TYR	11	HD*	VAL	24	HG*	4.06
TYR	11	HE*	VAL	24	HB	3.64
TYR	11	HE*	VAL	24	HG*	4.95
TYR	11	HN	VAL	24	HG*	4.24
TYR	11	HE*	ALA	25	HA	4.11
TYR	11	HE*	ALA	25	HB*	3.53
TYR	11	HD*	LEU	28	HD*	4.61
TYR	11	HE*	LEU	28	HD*	4.05
TYR	11	HD*	ALA	38	HB*	3.91
ALA	12	HN	LEU	8	HA	3.38
ALA	12	HB*	LYS	9	HA	3.26
ALA	12	HN	LYS	9	HA	3.21
ALA	12	HN	ALA	10	HN	4.27
ALA	12	HN	TYR	11	HB*	2.74
ALA	12	HN	TYR	11	HD*	3.50
ALA	12	HN	ALA	12	HA	2.82
ALA	12	HN	ALA	12	HB*	2.86
ALA	12	HN	GLU	13	HN	2.72
HIS	27	HD2	CYS	34	HA	3.82
HIS	27	HD2	CYS	34	HB*	2.69
LEU	28	HN	VAL	3	HG*	5.28
LEU	28	HN	VAL	24	HA	3.86
LEU	28	HN	VAL	24	HG*	5.10
LEU	28	HD*	ALA	25	HA	3.86
LEU	28	HG	ALA	25	HA	2.50
LEU	28	HN	ALA	25	HA	3.15
LEU	28	HN	LYS	26	HN	3.93
LEU	28	HN	HIS	27	HA	3.81
LEU	28	HN	HIS	27	HB*	2.99
LEU	28	HN	HIS	27	HD2	3.96
LEU	28	HN	HIS	27	HN	2.64
LEU	28	HB*	LEU	28	HA	2.84
LEU	28	HD*	LEU	28	HA	2.99
LEU	28	HD*	LEU	28	HB*	3.61
LEU	28	HN	LEU	28	HA	2.80
LEU	28	HN	LEU	28	HB*	3.25
LEU	28	HN	LEU	28	HD*	3.73
LEU	28	HN	LEU	28	HG	2.24
LEU	28	HN	SER	29	HN	2.73
LEU	28	HN	LYS	30	HN	4.22
LEU	28	HD*	CYS	31	HB*	5.58
LEU	28	HD*	CYS	34	HA	4.76
LEU	28	HD*	CYS	34	HB*	3.54
LEU	28	HD*	LYS	35	HB*	5.32
LEU	28	HD*	ALA	38	HB*	3.82
SER	29	HN	ALA	25	HA	3.73
SER	29	HN	LYS	26	HA	2.68
SER	29	HN	LEU	28	HA	3.16
SER	29	HN	LEU	28	HB*	4.02
SER	29	HN	LEU	28	HD*	4.75
SER	29	HN	SER	29	HA	2.65
SER	29	HN	SER	29	HB*	2.70
SER	29	HN	LYS	30	HN	2.64
LYS	30	HN	HIS	27	HA	3.51
LYS	30	HN	LEU	28	HA	3.53
LYS	30	HN	SER	29	HA	3.34
LYS	30	HN	SER	29	HB*	3.70
LYS	30	HB*	LYS	30	HA	2.62
LYS	30	HN	LYS	30	HB*	2.83
LYS	30	HN	LYS	30	HG*	3.25
LYS	30	HN	CYS	31	HB*	3.81
CYS	31	HB*	LEU	28	HA	3.43
CYS	31	HN	LEU	28	HA	3.03
CYS	31	HN	LYS	30	HB*	3.39
CYS	31	HN	LYS	30	HN	2.20
CYS	31	HB*	CYS	31	HA	2.63
CYS	31	HN	CYS	31	HB*	2.61
CYS	31	HB*	CYS	34	HB*	3.12
GLU	32	HN	CYS	31	HA	2.24
GLU	32	HN	CYS	31	HB*	3.98
GLU	32	HN	CYS	31	HN	3.83
GLU	32	HN	GLU	32	HA	2.83
GLU	32	HN	GLU	32	HB*	2.71
GLU	32	HN	GLU	32	HG*	3.21
GLU	32	HN	GLU	33	HN	2.74
GLU	33	HN	CYS	31	HA	3.22
GLU	33	HN	CYS	31	HN	4.25
GLU	33	HN	GLU	32	HB*	2.56

ALA	12	HN	GLY	14	HN	3.85
ALA	12	HN	VAL	24	HG*	5.41
ALA	12	HN	LEU	41	HD*	5.22
GLU	13	HN	ALA	12	HA	3.36
GLU	13	HN	ALA	12	HB*	3.01
GLU	13	HG*	GLU	13	HA	3.46
GLU	13	HN	GLU	13	HA	2.74
GLU	13	HN	GLU	13	HB*	2.60
GLU	13	HN	GLU	13	HG*	2.79
GLU	13	HN	GLY	14	HN	2.54
GLY	14	HN	GLU	13	HA	2.79
GLY	14	HN	GLY	14	HA*	2.53
THR	15	HG*	ALA	10	HA	4.48
THR	15	HN	ALA	10	HA	2.81
THR	15	HN	ALA	10	HB*	3.71
THR	15	HG2*	GLU	13	HB*	3.73
THR	15	HN	GLY	14	HA1	2.98
THR	15	HN	GLY	14	HN	2.55
THR	15	HG2*	THR	15	HA	3.04
THR	15	HN	THR	15	HA	2.81
THR	15	HN	THR	15	HB	3.37
THR	15	HN	THR	15	HG2*	3.28
THR	15	HN	LEU	16	HG	2.93
THR	15	HN	LEU	16	HN	2.46
LEU	16	HD*	ALA	10	HB*	4.00
LEU	16	HN	ALA	10	HB*	4.20
LEU	16	HD*	TYR	11	HA	3.10
LEU	16	HD*	TYR	11	HB*	3.98
LEU	16	HN	TYR	11	HA	3.21
LEU	16	HN	THR	15	HA	3.11
LEU	16	HN	THR	15	HG2*	4.51
LEU	16	HB*	LEU	16	HA	2.60
LEU	16	HD*	LEU	16	HA	3.67
LEU	16	HN	LEU	16	HA	2.80
LEU	16	HN	LEU	16	HD*	4.05
LEU	16	HD*	TYR	20	HA	4.33
LEU	16	HD*	TYR	20	HB*	3.47
LEU	16	HD*	SER	21	HA	3.70
SER	17	HN	ALA	10	HB*	4.57
SER	17	HN	LEU	16	HA	2.29
SER	17	HN	LEU	16	HB*	2.91
SER	17	HN	LEU	16	HD*	3.75
SER	17	HN	LEU	16	HN	3.84
SER	17	HN	SER	17	HA	2.89
SER	17	HN	SER	17	HB*	2.79
SER	17	HN	TYR	20	HB*	3.48
SER	17	HN	TYR	20	HD*	4.85
SER	17	HN	TYR	20	HN	3.88
GLU	18	HN	SER	17	HA	2.66
GLU	18	HN	SER	17	HB*	3.46
GLU	18	HN	SER	17	HN	4.53
GLU	18	HN	GLU	18	HA	2.75
GLU	18	HN	GLU	18	HB*	2.94
GLU	18	HN	GLU	18	HG*	3.99
GLU	18	HN	ALA	19	HB*	5.19
GLU	18	HN	ALA	19	HN	3.64
ALA	19	HN	GLU	18	HA	3.24
ALA	19	HN	GLU	18	HB*	3.19
ALA	19	HN	ALA	19	HA	2.82
ALA	19	HN	ALA	19	HB*	3.02
GLU	33	HN	GLU	33	HA	2.65
GLU	33	HN	GLU	33	HB*	3.21
CYS	34	HN	LEU	8	HD*	6.05
CYS	34	HN	HIS	27	HD2	3.93
CYS	34	HB*	LEU	28	HA	3.53
CYS	34	HN	LEU	28	HD*	5.03
CYS	34	HN	CYS	31	HA	3.94
CYS	34	HN	CYS	31	HB*	3.47
CYS	34	HN	GLU	32	HN	4.15
CYS	34	HN	GLU	33	HA	3.42
CYS	34	HN	GLU	33	HB*	3.14
CYS	34	HN	GLU	33	HG*	4.09
CYS	34	HN	GLU	33	HN	2.36
CYS	34	HB*	CYS	34	HA	2.67
CYS	34	HN	CYS	34	HA	2.77
CYS	34	HN	CYS	34	HB*	2.65
CYS	34	HN	LYS	35	HA	3.88
CYS	34	HN	ALA	36	HN	4.02
CYS	34	HN	LYS	37	HN	4.25
LYS	35	HN	LEU	28	HD*	4.33
LYS	35	HN	GLU	32	HA	2.69
LYS	35	HN	CYS	34	HB*	3.08
LYS	35	HB*	LYS	35	HA	2.91
LYS	35	HN	LYS	35	HA	2.69
LYS	35	HN	LYS	35	HB*	2.46
LYS	35	HN	LYS	35	HG*	3.80
LYS	35	HN	ALA	36	HN	2.67
LYS	35	HN	LYS	37	HN	3.77
ALA	36	HN	GLU	32	HA	3.15
ALA	36	HB*	GLU	33	HA	2.89
ALA	36	HN	GLU	33	HA	3.77
ALA	36	HN	LYS	35	HA	3.18
ALA	36	HN	LYS	35	HB*	2.73
ALA	36	HN	ALA	36	HA	2.87
ALA	36	HN	ALA	36	HB*	2.79
ALA	36	HN	LYS	37	HN	2.73
LYS	37	HN	LEU	8	HD*	4.84
LYS	37	HN	ALA	36	HA	3.12
LYS	37	HN	ALA	36	HB*	3.34
LYS	37	HN	LYS	37	HB*	2.92
LYS	37	HN	LYS	37	HG*	2.91
LYS	37	HN	ALA	38	HB*	4.17
ALA	38	HN	LEU	28	HD*	4.51
ALA	38	HB*	LYS	35	HA	3.24
ALA	38	HN	LYS	35	HA	3.19
ALA	38	HN	LYS	37	HB*	2.83
ALA	38	HN	LYS	37	HB*	2.92
ALA	38	HN	LYS	37	HN	3.01
ALA	38	HN	ALA	38	HA	2.41
ALA	38	HN	ALA	38	HB*	2.89
ALA	38	HN	GLN	39	HN	2.67
ALA	38	HN	LYS	40	HN	3.86
GLN	39	HN	ALA	36	HA	2.72
GLN	39	HN	ALA	36	HB*	4.05
GLN	39	HN	ALA	38	HB*	3.26
GLN	39	HN	GLN	39	HA	2.59
GLN	39	HN	GLN	39	HB*	2.66
GLN	39	HN	GLN	39	HB*	3.11
GLN	39	HN	LYS	40	HN	2.70
LYS	40	HN	LYS	37	HA	2.95

ALA	19	HB*	TYR	20	HA	4.55		LYS	40	HN	GLN	39	HA	3.20
ALA	19	HN	TYR	20	HN	2.92		LYS	40	HN	GLN	39	HB*	3.05
TYR	20	HD*	LEU	7	HD*	4.96		LYS	40	HN	LYS	40	HA	2.67
TYR	20	HE*	LEU	7	HD*	5.26		LYS	40	HN	LYS	40	HB*	2.64
TYR	20	HB*	LEU	16	HA	3.92		LEU	41	HD*	LEU	8	HB*	3.72
TYR	20	HD*	LEU	16	HD*	5.00		LEU	41	HD*	LYS	9	HA	3.59
TYR	20	HN	LEU	16	HD*	5.18		LEU	41	HD*	LYS	9	HE*	5.15
TYR	20	HN	GLU	18	HA	3.41		LEU	41	HD*	ALA	12	HB*	4.49
TYR	20	HD*	ALA	19	HB*	5.02		LEU	41	HD*	ALA	38	HA	3.77
TYR	20	HN	ALA	19	HB*	3.36		LEU	41	HN	ALA	38	HA	2.78
TYR	20	HB*	TYR	20	HA	2.68		LEU	41	HD*	LEU	41	HA	3.61
TYR	20	HD*	TYR	20	HA	3.90		LEU	41	HD*	LEU	41	HB*	4.00
TYR	20	HD*	TYR	20	HB*	4.34		LEU	41	HN	LEU	41	HA	2.66
TYR	20	HN	TYR	20	HA	2.85		LEU	41	HN	LEU	41	HB*	3.05
TYR	20	HN	TYR	20	HB*	2.70		LEU	41	HN	LEU	41	HD*	3.55
TYR	20	HN	TYR	20	HD*	4.25		LEU	41	HN	LEU	41	HG	2.29
TYR	20	HD*	VAL	24	HG*	5.68		LYS	42	HN	LEU	41	HA	4.31
SER	21	HN	TYR	11	HD*	5.06		LYS	42	HN	LYS	42	HA	2.77
SER	21	HN	LEU	16	HD*	4.48		LYS	42	HN	ALA	45	HB*	4.18
SER	21	HN	LEU	16	HN	4.85		ALA	43	HN	GLN	39	HA	3.55
SER	21	HN	SER	17	HN	4.43		ALA	43	HB*	LYS	40	HA	2.79
SER	21	HN	ALA	19	HA	3.73		ALA	43	HN	LYS	42	HA	2.98
SER	21	HN	ALA	19	HB*	4.87		ALA	43	HN	LYS	42	HB*	3.20
SER	21	HN	ALA	19	HN	4.21		ALA	43	HN	ALA	43	HA	3.08
SER	21	HN	TYR	20	HA	3.35		ALA	43	HN	ALA	43	HB*	3.44
SER	21	HN	TYR	20	HB*	3.19		LYS	44	HN	LYS	40	HA	3.33
SER	21	HN	TYR	20	HD*	5.66		LYS	44	HN	LEU	41	HA	3.33
SER	21	HN	TYR	20	HN	2.54		LYS	44	HN	LEU	41	HD*	5.00
SER	21	HN	SER	21	HA	2.82		LYS	44	HN	LYS	44	HA	2.52
SER	21	HN	SER	21	HB*	2.74		LYS	44	HN	LYS	44	HB*	2.53
SER	21	HN	LYS	22	HN	2.84		ALA	45	HB*	LEU	41	HA	2.86
SER	21	HN	LYS	23	HN	4.00		ALA	45	HN	LEU	41	HA	2.95
SER	21	HN	VAL	24	HG*	6.08		ALA	45	HN	LYS	44	HA	2.69
SER	21	HN	VAL	24	HN	4.62		ALA	45	HN	LYS	44	HB*	3.31
LYS	22	HN	TYR	20	HN	3.80		ALA	45	HN	ALA	45	HA	2.87
LYS	22	HN	LYS	22	HA	2.59		ALA	45	HN	ALA	45	HB*	2.87
LYS	22	HN	LYS	22	HB*	2.63		ALA	46	HN	ALA	46	HB*	3.65

Table S4 Dihedral angle restraints (°) used in calculations with X-PLOR for Zn·L$_{ASD}$(HHCC).

VAL	3	C	SER	4	N	SER	4	CA	SER	4	C	-65	-90	-40
SER	4	C	LYS	5	N	LYS	5	CA	LYS	5	C	-65	-90	-40
LYS	5	C	GLN	6	N	GLN	6	CA	GLN	6	C	-65	-90	-40
LEU	7	C	LEU	8	N	LEU	8	CA	LEU	8	C	-65	-90	-40
SER	8	C	LYS	9	N	LYS	9	CA	LYS	9	C	-65	-90	-40
LYS	9	C	ALA	10	N	ALA	10	CA	ALA	10	C	-65	-90	-40
ALA	10	C	TYR	11	N	TYR	11	CA	TYR	11	C	-65	-90	-40
TYR	11	C	ALA	12	N	ALA	12	CA	ALA	12	C	-65	-90	-40
GLY	14	C	THR	15	N	THR	15	CA	THR	15	C	-120	-160	-80
LEU	16	C	SER	17	N	SER	17	CA	SER	17	C	-65	-90	-40
SER	17	C	GLU	18	N	GLU	18	CA	GLU	18	C	-65	-90	-40
GLU	18	C	ALA	19	N	ALA	19	CA	ALA	19	C	-65	-90	-40
TYR	20	C	SER	21	N	SER	21	CA	SER	21	C	-65	-90	-40
SER	21	C	LYS	22	N	LYS	22	CA	LYS	22	C	-65	-90	-40
LYS	22	C	LYS	23	N	LYS	23	CA	LYS	23	C	-65	-90	-40
LYS	23	C	VAL	24	N	VAL	24	CA	VAL	24	C	-65	-90	-40
VAL	24	C	ALA	25	N	ALA	25	CA	ALA	25	C	-65	-90	-40
ALA	25	C	LYS	26	N	LYS	26	CA	LYS	26	C	-65	-90	-40
LYS	26	C	HIS	27	N	HIS	27	CA	HIS	27	C	-65	-90	-40
HIS	27	C	LEU	28	N	LEU	28	CA	LEU	28	C	-65	-90	-40

LEU	28	C	SER	29	N	SER	29	CA	SER	29	C	-65	-90	-40
SER	29	C	LYS	30	N	LYS	30	CA	LYS	30	C	-120	-160	-80
LYS	30	C	CYS	31	N	CYS	31	CA	CYS	31	C	-120	-160	-80
CYS	31	C	GLU	32	N	GLU	32	CA	GLU	32	C	-65	-90	-40
GLU	33	C	CYS	34	N	CYS	34	CA	CYS	34	C	-65	-90	-40
CYS	34	C	LYS	35	N	LYS	35	CA	LYS	35	C	-65	-90	-40
LYS	35	C	ALA	36	N	ALA	36	CA	ALA	36	C	-65	-90	-40
ALA	36	C	LYS	37	N	LYS	37	CA	LYS	37	C	-65	-90	-40
LYS	37	C	ALA	38	N	ALA	38	CA	ALA	38	C	-65	-90	-40
GLN	39	C	LYS	40	N	LYS	40	CA	LYS	40	C	-65	-90	-40
LYS	40	C	LEU	41	N	LEU	41	CA	LEU	41	C	-65	-90	-40
LEU	41	C	LYS	42	N	LYS	42	CA	LYS	42	C	-65	-90	-40
LYS	42	C	ALA	43	N	ALA	43	CA	ALA	43	C	-65	-90	-40
ALA	43	C	LYS	44	N	LYS	44	CA	LYS	44	C	-65	-90	-40
LYS	44	C	ALA	45	N	ALA	45	CA	ALA	45	C	-65	-90	-40

References

[1] G. Schwarzenbach, H. Flaschka, *Complexometric Titrations*, Methuen, London, **1969**.
[2] P. W. Riddles, R. L. Blakeley, B. Zerner, *Methods Enzymol.* **1983**, *91*, 49–60.
[3] E. Bourlès, M. Isaac, C. Lebrun, J.-M. Latour, O. Sénèque, *Chem.-Eur. J.* **2011**, *17*, 13762–13772.
[4] K. Mikkelsen, S. Nielsen, *J. Phys. Chem.* **1960**, *64*, 632–637.
[5] V. Lebrun, A. Tron, L. Scarpantonio, C. Lebrun, J.-L. Ravanat, J.-M. Latour, N. D. McClenaghan, O. Sénèque, *Angew. Chem., Int. Ed.* **2014**, *53*, 9365–9368.
[6] V. Lebrun, A. Tron, C. Lebrun, J.-M. Latour, N. D. McClenaghan, O. Sénèque, *Chem.-Eur. J.* **2015**, *21*, 14002–14010.
[7] V. Sklenar, M. Piotto, R. Leppik, V. Saudek, *J. Magn. Reson. Ser. A* **1993**, *102*, 241–245.
[8] M. Piotto, V. Saudek, V. Sklenar, *J. Biomol. NMR* **1992**, *2*, 661–665.
[9] T. D. Goddard, D. G. Kneller, *SPARKY 3.1*, University of California, San Francisco, **n.d.**
[10] A. T. Brünger, *A System for X-Ray Crystallography and NMR. X-PLOR, Version 3.1*, Yale University Press, New Haven, **1992**.